Scleraxis-Lineage Cell Depletion Improves Tendon Healing and Disrupts Adult Tendon Homeostasis

Authors: Katherine T. Best[1], Antonion Korcari[1,2], Keshia E. Mora[1,2], Emma Knapp[1], Mark R. Buckley[1,2], Alayna E. Loiselle[1,2*]

Affiliations

[1]Center for Musculoskeletal Research, University of Rochester Medical Center, Rochester, NY 14642, United States of America

[2]Department of Biomedical Engineering, University of Rochester, Rochester, New York, United States of America.

***Corresponding author**

Alayna E. Loiselle, PhD

Center for Musculoskeletal Research

University of Rochester Medical Center

601 Elmwood Ave

Box 665

Rochester, NY

14642

Phone: 585-275-7239

Fax: 585-276-2177

Alayna_Loiselle@urmc.rochester.edu

Conflict of Interest Statement: The authors have declared that no conflict of interest exists.

Abstract

Despite the requirement for *Scleraxis*-lineage (Scx^{Lin}) cells during tendon development, the function of Scx^{Lin} cells during adult tendon repair, post-natal growth, and adult homeostasis have not been defined. Therefore, we inducibly depleted Scx^{Lin} cells ($ScxLin^{DTR}$) prior to tendon injury and repair surgery and hypothesized that $ScxLin^{DTR}$ mice would exhibit functionally deficient healing compared to wildtype littermates. Surprisingly, depletion of Scx^{Lin} cells resulted in increased biomechanical properties without impairments in gliding function at 28 days post-repair, indicative of regeneration. RNA sequencing of day 28 post-repair tendons highlighted differences in matrix-related genes, cell motility, cytoskeletal organization, and metabolism. We also utilized $ScxLin^{DTR}$ mice to define the effects on post-natal tendon growth and adult tendon homeostasis and discovered that adult Scx^{Lin} cell depletion resulted in altered tendon collagen fibril diameter, density, and dispersion. Collectively, these findings enhance our fundamental understanding of tendon cell localization, function, and fate during healing, growth, and homeostasis.

Introduction

Despite the significant efforts toward improving tendon healing and regeneration, the specific cellular contributions during tendon healing have not been extensively characterized[1]. While many studies have examined the potential of using various stem cell populations to promote healing, originating from both tendon intrinsic[2] and extrinsic sources[3], little focus has been directed toward defining the functions and therapeutic potential of tendon cells during tendon healing following an acute injury. Tendon cells are increasingly recognized as a heterogenous population of cells where many, but not all, express the gene *Scleraxis* (*Scx*)[4-6]. Understanding the localization and function of tendon cell subpopulations during healing is likely to be instrumental in better defining the mechanisms that promote scar-mediated healing, which results in poor patient outcomes, and could therefore be used to develop pro-regenerative approaches to improve healing.

Scx, a basic helix-loop-helix transcription factor, is currently the most well-characterized marker that the field possesses to study tendon[7]. *Scx* has been utilized to examine tendon biology and development[8-10], healing and regeneration[4,11-13], differentiation[14-17], and mechano-transduction[18,19]. Functionally, *Scx* expression can drive matrix production and remodeling[11,20,21], epithelial-to-mesenchymal transition[22], development of force-transmitting tendons[8], tendon growth[23], and effect focal adhesion morphology[19]. Despite the effort to understand the functions of *Scx* as a transcription factor, the function and requirement of *Scx*-lineage (Scx^{Lin}) cells in tendon repair, post-natal growth and homeostasis has not been defined.

Previous studies examining the localization and role of tendon cells during healing are limited. *Scx*-GFP mice[24] have been used to visualize tendon cells in many studies; however, previous work has suggested that extrinsic, paratenon-derived *Scx*-GFP^- cells can turn on *Scx* expression and become *Scx*-GFP^+ by 14 days in Patellar tendon injury model[13]. This makes interpretation using *Scx*-GFP mice complicated during *in vivo* studies as it becomes difficult to determine if a *Scx*-GFP^+ cell is tendon-derived or simply activating *Scx* expression post-injury. Other studies have utilized the inducible Scx-Cre^{ERT2} mouse to label Scx^+ cells prior to injury to allow tracking of these cells post-injury (Scx^{Ai9}). Howell *et al*. determined that while *Scx*-GFP cells and Scx^{Ai9} tendon cells localized to the regenerated tendon in neonatal mice, these cells were not recruited to the

scar tissue/bridging tissue during adult healing in Achilles tendon[12]. In contrast, we have previously demonstrated that Scx^{Ai9} tendon cells organize into a linear, cellular bridge spanning the scar tissue between the tendon stubs following acute injury and repair of the adult flexor digitorum longus tendon[4]. While these studies suggest that tendon type (ex. flexor, Achilles, etc.) and injury model-specific (ex. transection with no repair, transection with repair, etc.) differences may modulate the Scx^{Lin} cell contribution to injury, it also highlights the near complete lack of characterization of Scx^{Lin} cell function in the healing process.

In the present study, we hypothesized that Scx^{Lin} tendon cells would be required for successful healing in an adult model of acute flexor tendon repair by driving formation of a collagenous tissue bridge. We utilized a genetic mouse model of Scx^{Lin} cell depletion to directly assess the function of tendon cells during healing and surprisingly discovered that depletion of Scx^{Lin} tendon cells resulted in improved tendon biomechanical properties. We also examined alterations in wound healing-related cell populations, transcriptomics via RNA sequencing, and the effects of Scx^{Lin} cell depletion on tendon post-natal growth and homeostasis.

Results

Successful ablation of *Scleraxis*-lineage tendon cells using diphtheria toxin receptor mouse model.

Scx^{Lin} cells account for ~80% of tendon cells in the flexor digitorum longus (FDL) tendon (Fig. 1A and B). To deplete tendon cells, Scx-Cre mice were crossed to diphtheria toxin receptor ($DTR^{F/F}$) animals ($ScxLin^{DTR}$) (Fig. 1C). Five local hind paw injections of diphtheria toxin (DT) (Fig. 1D) resulted in 57% depletion of tendon cells in uninjured $ScxLin^{DTR}$ FDL tendons relative to WT control littermates ($p < 0.0001$) (Fig. 1E and F). Tendon cell number was unaffected in the contralateral FDL, indicating that local DT injections did not induce cell death in locations other than the targeted hind paw (Fig. 1E and F). To understand how $ScxLin^{DTR}$ affected previously established tendon cell sub-populations[4], we evaluated active Scx and S100a4 expression in $ScxLin^{DTR}$ and WT uninjured flexor tendons 10 days following the final DT injection. The number of Scx+ cells was significantly reduced in the $ScxLin^{DTR}$ tendons relative to WT littermates, as expected ($p=0.0448$) (Fig. 1-Figure Supplement 1A &B). Similarly, when Scx+ cells were normalized to total cell count, there was a trending reduction of Scx+ cells in $ScxLin^{DTR}$ tendons compared to WT ($p=0.1000$) (Fig. 1- Figure Supplement 1C). $ScxLin^{DTR}$ tendons had a trending decrease in S100a4+ cells relative to WT littermates ($p=0.0941$) (Fig. 1-Figure Supplement 1D &E). Interestingly, when S100a4+ cells were normalized to total cell count, there was no significant or trending difference between groups ($p=0.3525$), suggesting some remaining tendon cells may begin expressing S100a4 following Scx^{Lin} depletion (Fig. 1- Figure Supplement 1F). $ScxLin^{DTR}$ tendons exhibited a small number of apoptotic cells peripheral to, but not within, the tendon suggesting that a 10-day DT washout period was sufficient for all tendon-specific DT-induced cell death to occur (Fig. 1- Figure Supplement 2A). Both $ScxLin^{DTR}$ and WT littermates exhibited PCNA+ cells within the muscle, but not within then tendon, and $ScxLin^{DTR}$ exhibited a few PCNA+ cells within the tendon that were not present in WT (Fig. 1- Figure Supplement 2B). $ScxLin^{DTR}$ tendons exhibited more F4/80+ macrophages peripheral to the tendon, potentially due to macrophage recruitment to the tendon to clean up apoptotic tendon cell debris (Fig. 1- Figure Supplement 2C).

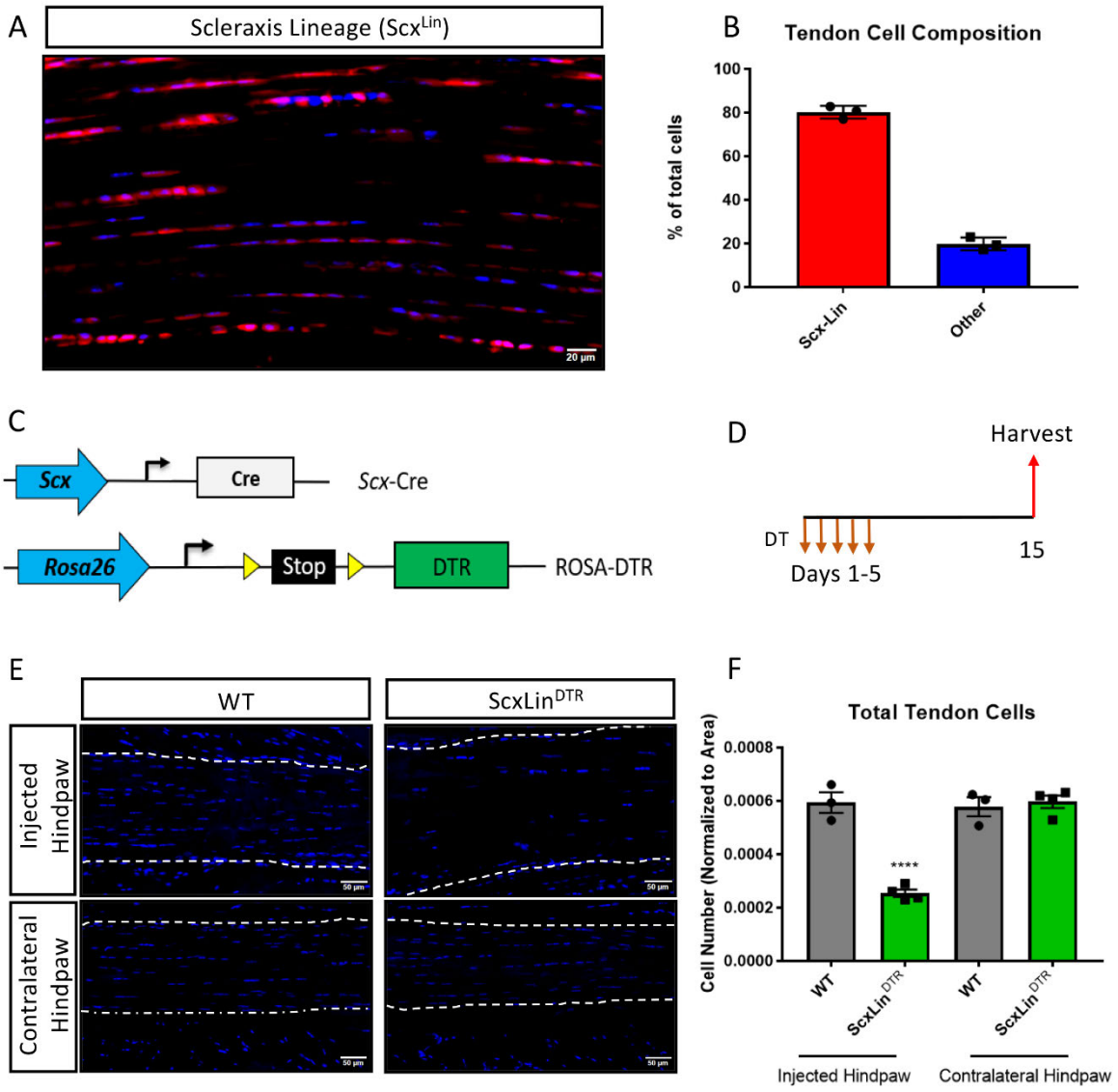

Figure 1. Model of Scleraxis lineage tendon cell depletion. Scx-Cre mice were crossed to ROSA-Ai9 reporter mice to trace (A) and quantify (B) *Scx* lineage cells (Scx^{Lin}) in uninjured flexor tendon. N=3. To deplete Scx^{Lin}, Scx-Cre mice were crossed to the diphtheria toxin receptor mouse ($ScxLin^{DTR}$, C). Mice received five hind paw injections of DT and were harvested ten days after the final injection (D). Hind paw sections from both WT and $ScxLin^{DTR}$ injected hind paws contralateral hind paws (E). Quantification of injured and contralateral hind paw tendon cell number (F). When needed, tendon outlined by white dotted line. Nuclei stained with DAPI. N=3-4 per genotype. 2-way ANOVA with Sidak's multiple comparisons test used to assess statistical significance of tendon cell ablation between hind paw (injected with DT or contralateral) and genotype (WT and $ScxLin^{DTR}$). **** indicates $p<0.0001$ relative to all other groups.

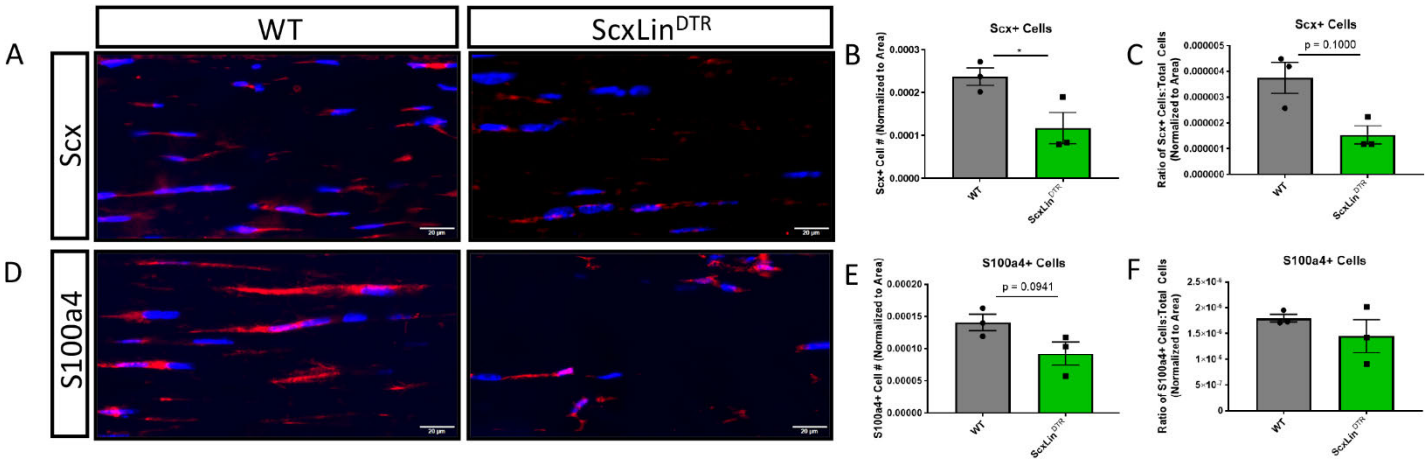

Figure 1 – Figure Supplement 1. *Scx*+ and *S100a4*+ tendon cells following Scx^{Lin} depletion. WT and ScxLin^{DTR} hind paws were harvested uninjured 10 days following final DT injection and stained for either *Scx* (A-C) or *S100a4* (D-F). Quantification of *Scx*+ cells normalized to either total area (B) or both area and total cell number (C). Quantification of *S100a4*+ cells normalized to either total area (E) or both area and total cell number (F). N=3 per genotype. Statistical significance between genotypes determined using Student's t-test when data was normal (B, E, F) or Mann-Whitney test when data not normal (C). * indicative of $p \leq 0.05$.

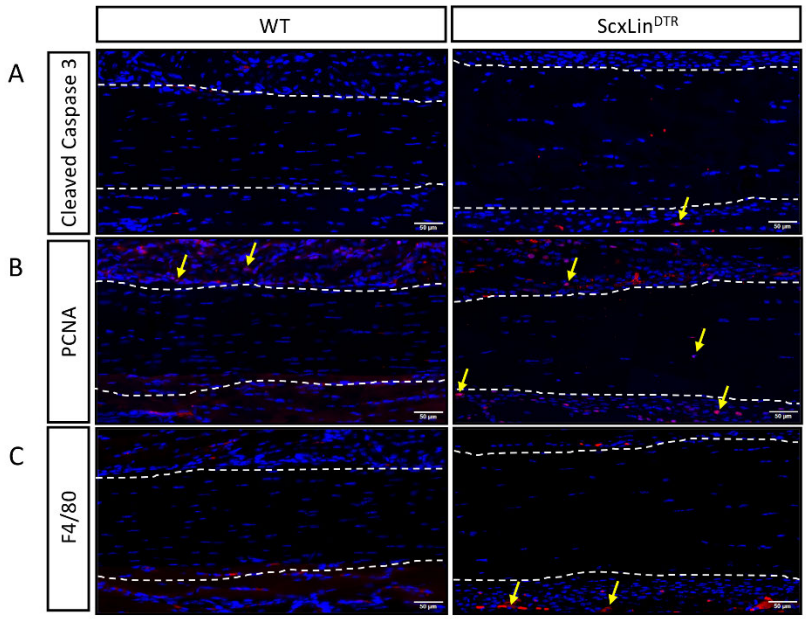

Figure 1 – Figure Supplement 2. ScxLin^{DTR} does not cause substantial effects on surrounding tissue. Assessment of apoptosis (Cleaved Caspase 3, A), proliferation (PCNA, B), and Inflammation (F4/80, macrophages, C) for WT and ScxLin^{DTR} uninjured tendons. Tendon outlined by white dotted line. Nuclei stained with DAPI. Examples of positive stain indicated by yellow arrows. N=3 per genotype.

Ablation of Scleraxis-lineage cells results in significantly increased biomechanical properties by day 28 post repair while not affecting gliding function.

To define the functional effects of Scx^{Lin} cell depletion on tendon healing, mice received five local DT injections to deplete Scx^{Lin} cells followed by FDL repair 10 days following the final injection (Fig. 2A). A trending improvement in MTP Range of Motion (ROM) in $ScxLin^{DTR}$ repairs was observed at day 14, relative to WT littermates (WT vs $ScxLin^{DTR}$, $p = 0.0711$), but this trend was absent by day 28 post-repair (Fig. 2B). $ScxLin^{DTR}$ healing tendons did not significantly differ in gliding resistance at either day 14 or 28 post-repair (Fig. 2C). While biomechanical properties were not altered between groups at day 14, both stiffness and maximum load at failure were significantly increased in $ScxLin^{DTR}$ healing tendons relative to wildtype littermates at day 28 post-repair (Stiffness: WT: 6.48 ± 0.75, $ScxLin^{DTR}$: 11.22 ± 1.83 , $p = 0.0237$; Maximum load at failure: WT: 1.54 ± 0.17, $ScxLin^{DTR}$: 2.44 ± 0.24 , $p = 0.0061$) (Fig. 2D and E). Between days 14 and 28, WT tendon stiffness increased by 39.06% while $ScxLin^{DTR}$ stiffness increased by 109.33%, and WT tendon maximum load at failure increased by 52.48% while $ScxLin^{DTR}$ maximum load at failure increased by 162.37%, indicating that $ScxLin^{DTR}$ repairs heal at an accelerated rate relative to wildtype littermates.

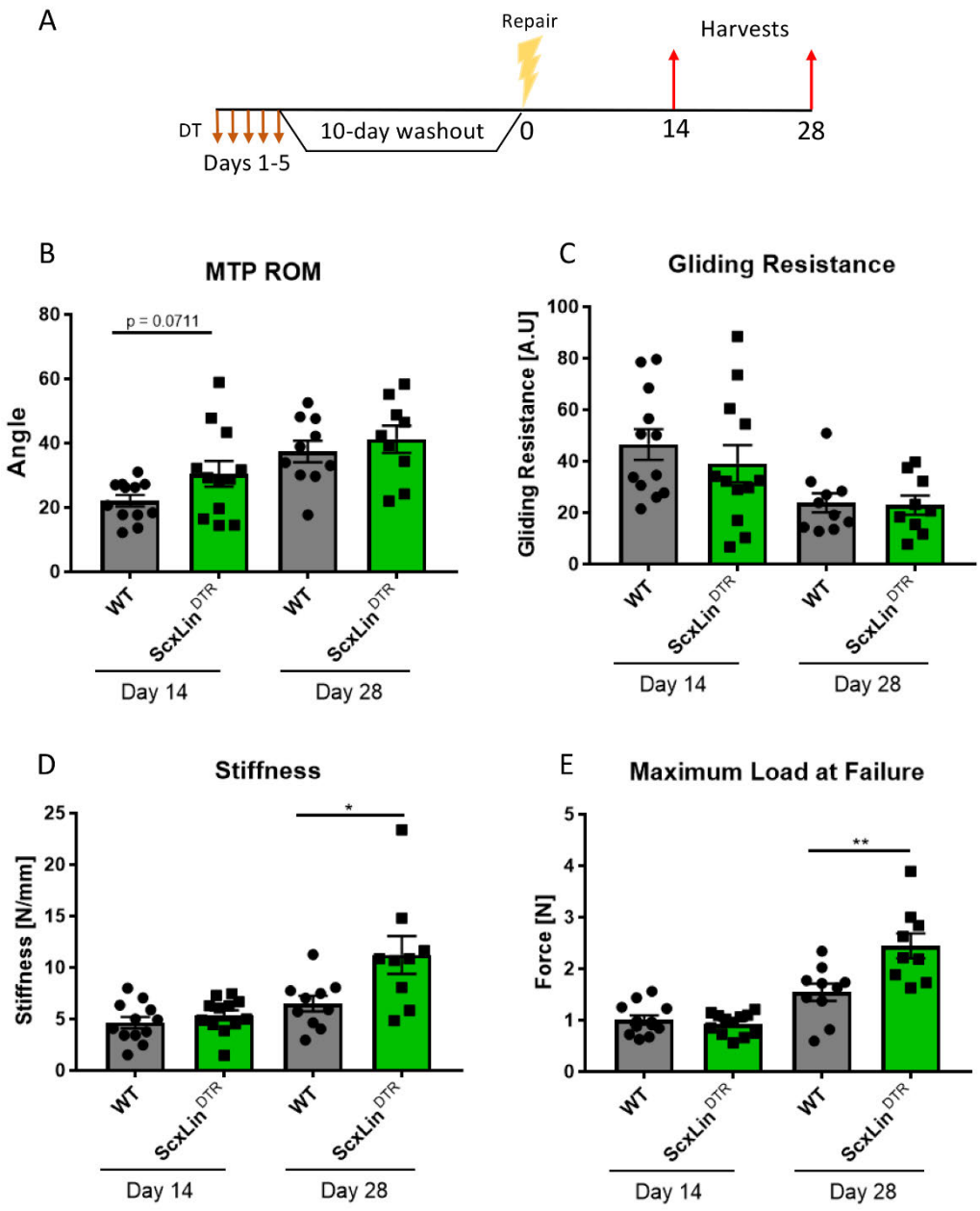

Figure 2. ScxLin^{DTR} tendons heal with significantly increased biomechanical properties. Mice received five hind paw injections of DT on consecutive days, underwent flexor tendon repair surgery ten days after the final DT injection, and were harvested at 14- and 28-days post-repair (A). Measurement of metatarsophalangeal (MTP) joint flexion angle (B), gliding resistance (C), stiffness (D), and maximum load at failure (E) of WT and ScxLin^{DTR} repaired tendons. N=9-12 per genotype per timepoint. Students t-test used to assess statistical significance between genotypes at a given timepoint. * indicative of $p < 0.05$, ** indicative of $p < 0.01$.

Scleraxis-lineage cells are not required for the formation of a bridging collagen matrix during tendon healing.

We have previously demonstrated that a cellular bridge corresponds to a region of bridging collagen matrix in the scar tissue[4]. While there were no apparent differences in tissue morphology between groups at days 14 or 28 post-repair (Fig. 3B), we wanted to determine if tendon cell depletion prevented formation of the collagen bridge. Masson's trichrome staining revealed presence of bridging collagen through the scar in both groups at days 14 and 28, indicating that depletion of Scx^{Lin} tendon cells does not prevent formation of the bridging collagen matrix (Fig. 3C).

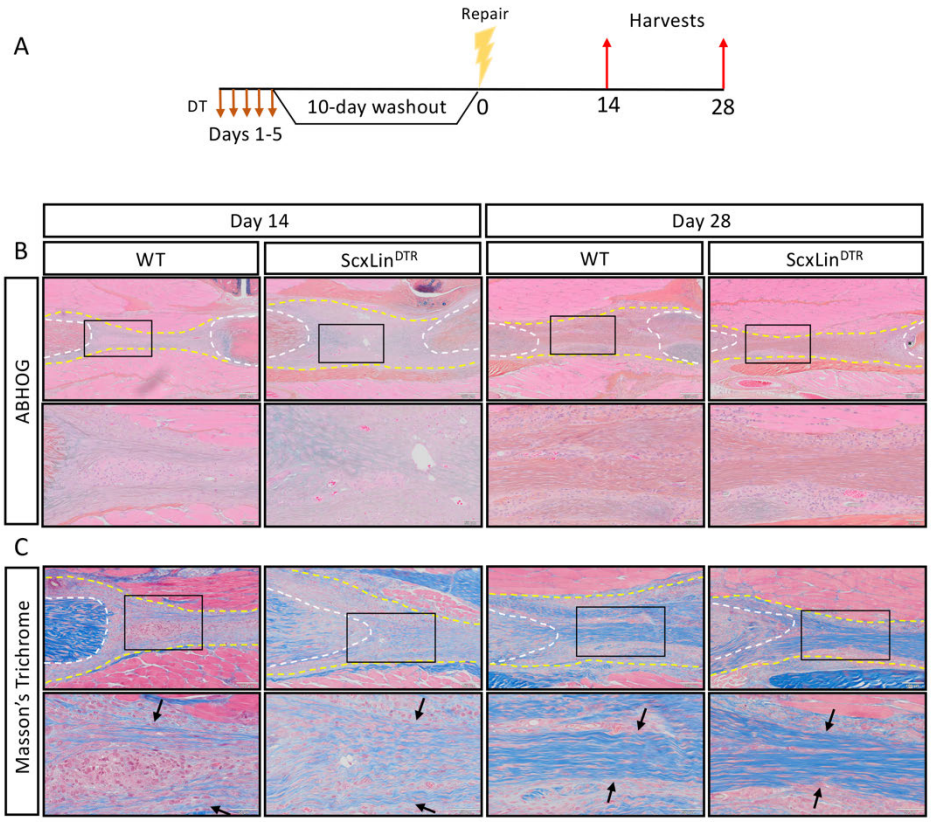

Figure 3. Scx^{Lin} cell depletion does not disrupt formation of a bridging collagen matrix. Mice received five hindpaw injections of DT on consecutive days, underwent flexor tendon repair surgery ten days after the final DT injection, and were harvested at 14 and 28 days post-repair (A). Alcian blue/hematoxylin and Orange G stain utilized to assess overall morphology (B). Masson's trichrome stain used to visualize collagen content and organization (C). Tendon is outlined by white dotted line and scar tissue by yellow dotted line. Black boxes indicate location of higher magnification images. Boundaries of bridging collagen indicated by black arrows. N=4 genotype per timepoint. Suture indicated by *.

Scx^{Lin} Depletion enhances myofibroblast content during tendon healing.

We have previously demonstrated that elevated F4/80+ macrophages and αSMA+ myofibroblasts are associated with increased tendon maximum load at failure[25]. No significant differences in F4/80+ macrophages were detected between genotypes at either day 14 or 28 post-repair (Fig. 4B). While αSMA+ myofibroblasts were not significantly altered at day 14 (D14: WT vs DTR, $p = 0.3790$), $ScxLin^{DTR}$ healing tendons had significantly increased levels of αSMA+ myofibroblasts relative to wildtype littermates at D28 ($p = 0.0188$) (Fig. 4C). We have previously demonstrated that S100a4 is an important molecule that can influence tendon biomechanical properties and gliding function during healing[26]. No differences in S100a4+ cells were observed in $ScxLin^{DTR}$, relative to WT at either day 14 or 28 post-repair (Fig. 4D). Thus, αSMA+ myofibroblasts are the most likely candidate driving the increased biomechanical properties seen in $ScxLin^{DTR}$ healing tendon, of the cell populations investigated, consistent with their roles in with matrix deposition, organization, and contraction.

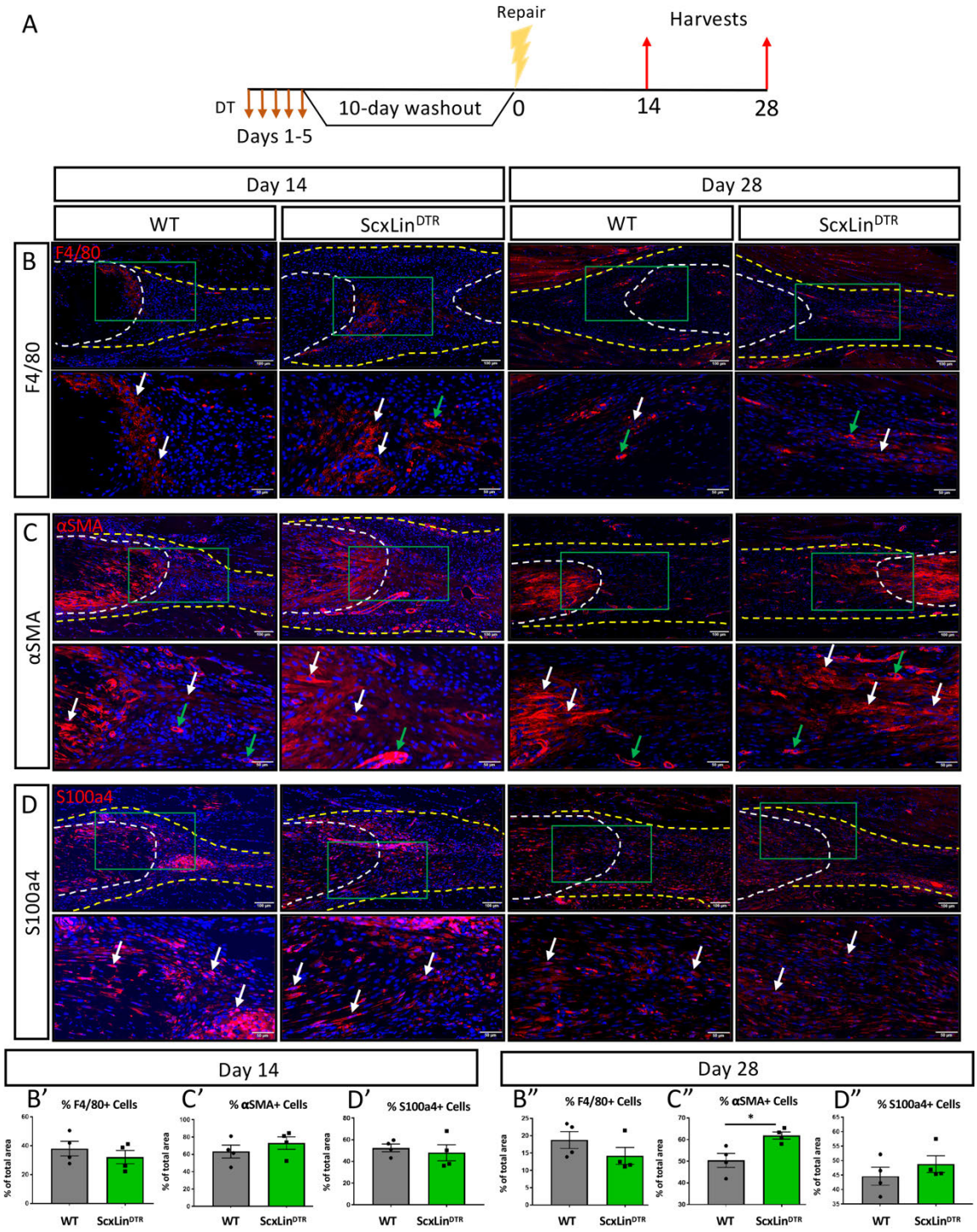

Figure 4. ScxLin^{DTR} repaired tendons heal with increased presence of αSMA+ myofibroblasts. Mice received five hindpaw injections of DT on consecutive days, underwent flexor tendon repair surgery ten days after the final DT injection, and were harvested at 14 and 28 days post-repair (A). Immunofluorescence of WT and ScxLin^{DTR} repair tendons 14 and 28-days post-repair to assess F4/80+ macrophages (B), αSMA+ myofibroblasts (C), and S100a4+ cells (D). Tendon is outlined by white dotted line and scar tissue by yellow dotted line. Green boxes indicate location of higher magnification images. Examples of positive stain indicated by white arrows, while examples of auto-fluorescent blood cells and α-SMA+ blood vessels indicated by green arrows. Quantification of F4/80 (A' & A''), αSMA (B' & B''), and S100a4 (C' & C'') fluorescence. N=4 per genotype per timepoint. Student's t-test used to assess statistical significance between genotypes at a given timepoint, except for D28 F4/80 and S100a4 which required a Mann-Whitney test. * indicates $p < 0.05$.

Identification of differentially expressed genes following Scx^{Lin} depletion.

To further investigate the mechanisms driving altered biomechanical properties of healing $ScxLin^{DTR}$ tendons, bulk RNAseq analysis was conducted on day 14 and 28 post-repair samples from $ScxLin^{DTR}$ and WT. A total of three biological replicates per genotype per timepoint were submitted for analysis. At 14 days post-repair, 47 genes were up-regulated, and 313 genes were down-regulated in $ScxLin^{DTR}$ relative to WT (Fig. 5A, B). At 28 days post-repair, 1237 genes were up-regulated, and 1296 genes were down-regulated in $ScxLin^{DTR}$ relative to WT (Fig. 5C, D). Based on both the low number of differentially expressed genes (DEGs) and the lack of mechanical phenotype at D14 between WT and $ScxLin^{DTR}$ (Fig. 2), our primary RNAseq analyses were focused on day 28.

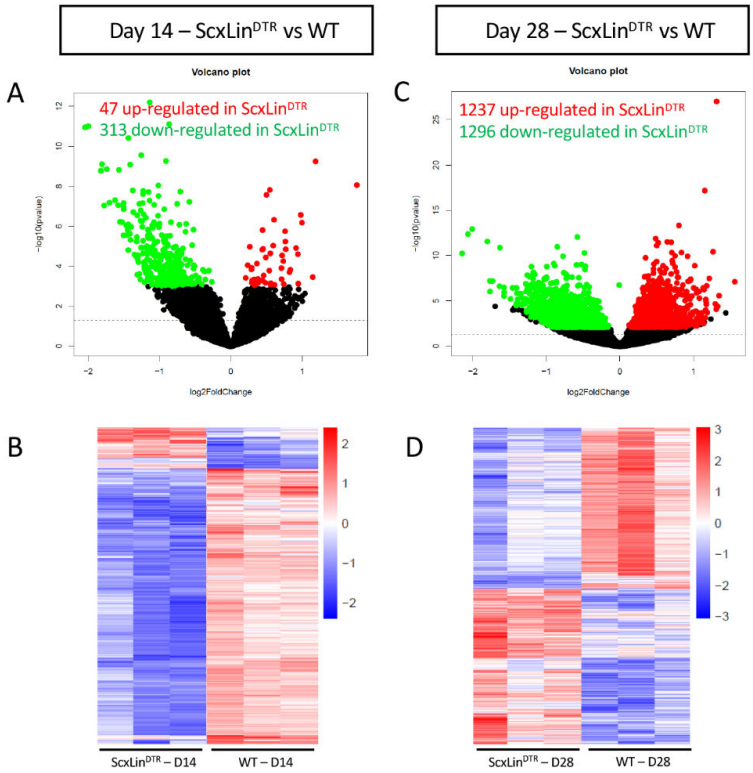

Figure 5. Bulk RNA sequencing reveals differences between $ScxLin^{DTR}$ and wildtype healing flexor tendons at 14 and 28 days post-repair. Representation of differentially expressed genes (DEGs) at 14 (A, B) and 28 (C, D) days post-repair. Volcano plots (A, C) depict significantly upregulated DEGs as red dots and significantly downregulated DEGs as green dots. DEGs are consider significant when the multiple test corrected (adjusted) p-value is ≤ 0.05. The dotted line represents the unadjusted p-value of 0.05. Heat maps (B, D) depict all significant DEGs, with the data representing the regularized log transformation of the normalized count data. N=3 biological replicates per genotype per time point.

Scx^{Lin} depletion drives differential expression of matrix-related gene expression.

The day 28 dataset was analyzed using ingenuity pathway analysis (IPA) software. We hypothesized that a change in the matrix composition could be driving the altered biomechanical properties detected at day 28 post-repair in $ScxLin^{DTR}$ animals, possibly driven by the elevated myofibroblast content. To examine the biological effects of Scx^{Lin} cell depletion at the transcriptional level, downstream effects analysis was performed by utilizing the core analysis in IPA where activation states were assigned for biological processes with p-value <0.05 and z-score ≥ 2 (Table 1). Included in the significantly increased disease and function annotations was "Fibrosis" (p = 3.37E-07, Z = 2.397, Table 1). As we have already demonstrated that depletion of Scx^{Lin} cells is not driving increased fibrotic healing (Fig. 2B, C), we then examined if the significantly increased "Fibrotic" annotation was indicative of altered expression of specific matrix-associated genes. Utilizing the comprehensive review of the matrisome by Hynes and Naba[27], genes coding for collagens, proteoglycans, basement membrane proteins, and glycoproteins were compiled and examined (Table 2). Many matrix-related genes were significantly increased in $ScxLin^{DTR}$ repairs relative to WT littermates at day 28 post-repair (ex. *Col1a2, Col3a1, Col8a1, Epyc, Thbs4,* complete list in Table 2), while other matrix components were significantly decreased (ex. *Col6a4, Col9a1, Fras1*, complete list in Table 2).

Effects on cell motility, cytoskeletal organization, metabolism, and oxidative stress identified in $ScxLin^{DTR}$ repair tendons.

Utilizing the downstream effects analysis described above (Table 1), we next examined other significantly altered biological functions in $ScxLin^{DTR}$ tendon repairs relative to WT. The inhibited pathways indicated decreased contractility and function of muscle (ex. "Contractility of skeletal muscle," p = 4.96E-16, Z = -3.595) and decreased oxygen consumption ("Consumption of Oxygen," p = 9.42E-07, Z = -2.237) in $ScxLin^{DTR}$ tendons relative to wildtype controls at day 28 post-repair (Table 1). While only 14 disease and function annotations were found to be inhibited, 62 annotations were found to be significantly activated. Interestingly, in addition to "Fibrosis," the activated biological pathways indicated increased cell movement and migration (ex.

"Migration of cells," p = 6.44E-17, Z = 4.733), reorganization of the cytoskeletal network (ex. "Organization of cytoskeleton," p = 2.94E-20, Z = 3.384), metabolism disorders (ex. "Glucose metabolism disorder," p = 5.46E-10, Z = 3.516), and production of reactive oxygen species (ex. "Production of reactive oxygen species," p = 6.22E-12, Z = 2.625) (Table 1).

Differentially enriched canonical pathways following Scx^{Lin} cell depletion prior to flexor tendon repair. To better understand signaling cascades that could be driving alterations in $ScxLin^{DTR}$ healing, enriched canonical pathways were identified using IPA core analysis. Nineteen canonical pathways were identified, where 13 were positively enriched (activated) and 6 were negatively enriched (inhibited/suppressed) (Fig. 6, Supplemental Table 1). Consistent with the metabolism disorders identified from the downstream effects analysis (Table 2), canonical pathways related to metabolism were negatively enriched (ex. "Oxidative Phosphorylation," -log(p) = 7.6, Z = -5.303; additional pathways provided in Fig. 6 and Supplemental Table 1). Additionally, calcium signaling was found to be negatively enriched ("Calcium Signaling," -log(p) = 5.72, Z = -2.335) (Fig. 6 and Supplemental Table 1).

Consistent with reorganization of the cytoskeletal network identified from the downstream effects analysis (Table 2), numerous canonical pathways related to actin nucleation and polymerization were positively enriched (Fig. 6 and Supplemental Table 1). These include "Rac Signaling" (-log(p) = 3.85, Z = 3.674), "RhoA Signaling" (-log (p) = 3.97, Z = 2.502), and "Ephrin B Signaling" (-log(p) = 3.09, Z = 2.53). Other pathways that are significantly enriched in $ScxLin^{DTR}$ day 28 post-repair tendons include, but are not limited to, "sphingosine-1-phosphate signaling" (-log(p) = 3.94, Z = 2.711) and "production of nitric oxide and reactive oxygen species in macrophages" (-log(p) = 2.01, Z = 2.117) (Fig. 6 and Supplemental Table 1).

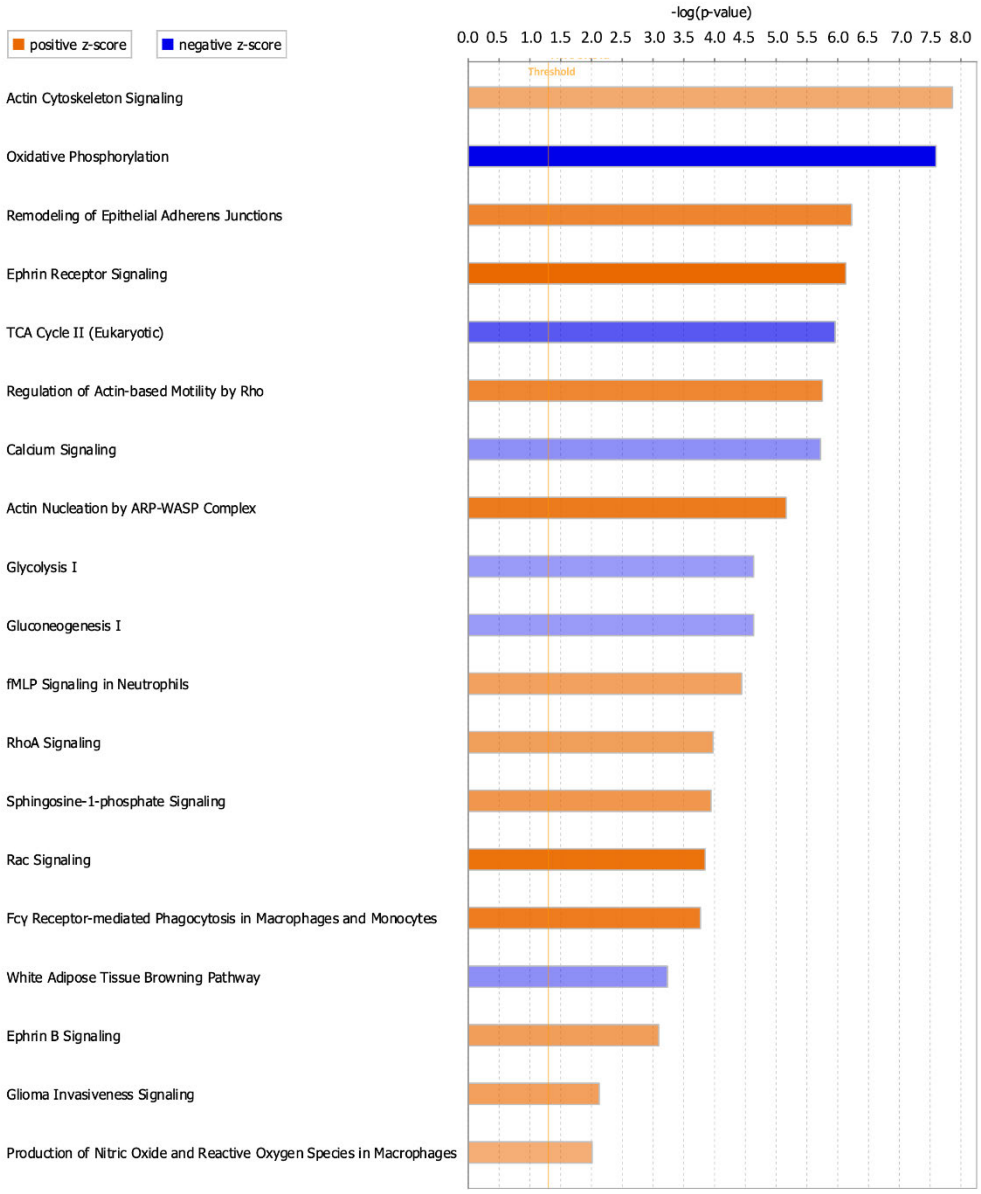

Figure 6. Canonical Pathways positively and negatively enriched in ScxLin^{DTR} healing tendons at day 28 post-repair. Ingenuity pathway analysis was utilized to determine positively and negatively significantly enriched pathways in ScxLin^{DTR} healing tendons at day 28 post-repair. Canonical pathways were considered significant if $p \leq 0.05$ and ABS(Z-score) ≥ 2. The orange color indicates pathways that are significantly, positively enriched ("activated"), while the blue color indicates significantly, negatively enriched ("inhibited") pathways. The orange dotted line represents -log (1.3) = 0.05, indicating the p-value cut-off. Data based on N=3 biological replicates per genotype.

Identification of possible upstream regulators driving altered ScxLin^{DTR} flexor tendon healing.

To identify key molecules that may be driving ScxLin^{DTR} tendon healing at day 28 post-repair, predicted upstream regulators were identified using IPA core analysis. Eight possible activated upstream regulators and four inhibited upstream regulators were identified (Table 3). The eight activated regulators included the calcium-binding protein S100a4, peptidase F2, receptors BTNL2 and F2R, transcription factors EBF2 and SOX2, the kinase NTRK2, and growth factor FGF2. The four inhibited regulators included enzyme LDHB and transcription factors FOXO4, MEF2C, and SMYD1.

Ablation of Scx^{Lin} tendon cells does not significantly affect tendon post-natal growth 3 months post-ablation.

In addition to roles in tendon healing, *Scx* expression is required for appropriate tendon development and growth processes[8,23]. However, the role of Scx+ cells during post-natal growth and adult homeostasis have not been evaluated. Local injection of DT into pre-pubescent mice (3-4 weeks old) resulted in 55% depletion of tendon cells in uninjured ScxLin^{DTR} FDL tendons relative to WT littermates ($p = 0.0007$) (Fig. 7A-C). To assess the requirement for tendon cells in post-natal growth, pre-pubescent mice who were still undergoing periods of rapid growth were injected with DT and harvested at the 3-month timepoint (ScxLin^{DTR,3weeks}) (Fig. 7D). ScxLin^{DTR,3weeks} tendons did not exhibit an influx of F4/80+ macrophages or tendon cell differentiation into αSMA+ myofibroblasts in either genotype (Fig. 7E); however, ScxLin^{DTR} mice had a 42.5% decreased tendon cell number relative to WT littermates ($p = 0.0454$) demonstrating that the Scx^{Lin} cells had not repopulated the tendon (Fig. 7E and F). There were no significant changes in MTP range of motion, gliding resistance, stiffness, or maximum load at failure between groups (Fig. 7G-J). Second harmonic generation revealed no significant differences in collagen fibril dispersion between genotypes (Fig. 7K and L). Taken together, these data suggest that Scx^{Lin} cells are not required for early post-natal tendon growth.

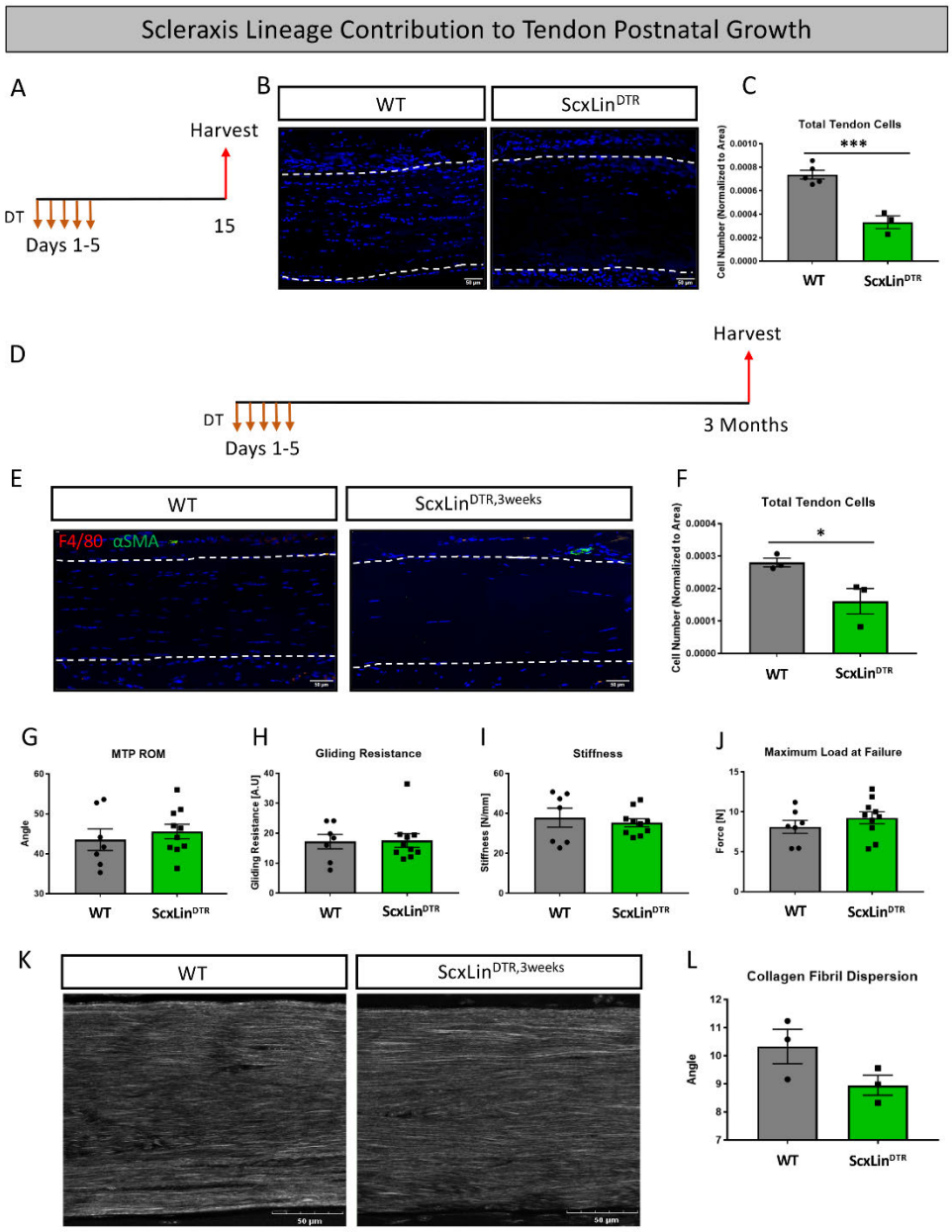

Figure 7. Tendon cell ablation does not negatively affect post-natal tendon growth 3 months post-ablation. Pre-pubescent mice (3-4 weeks old) received five hindpaw injections of DT and were harvested ten days after the final injection to assess tendon cell depletion ($ScxLin^{DTR}$) (A). Hindpaw sections from both WT and $ScxLin^{DTR}$ hindpaws (B). Quantification of WT and $ScxLin^{DTR,3weeks}$ tendon cell number in pre-pubescent mice (C). N=3-5 per genotype. To assess effects of tendon cell depletion on post-natal tendon growth, mice received five hindpaw injections of DT on consecutive days at 3-4 weeks of age and were harvested uninjured 3 months later for biomechanical, gliding, and histological evaluation ($ScxLin^{DTR,3weeks}$) (D). Co-immunofluorescence of F4/80 (macrophages) and αSMA (myofibroblasts) in uninjured WT and $ScxLin^{DTR,3weeks}$ tendons (E). Quantification of WT and $ScxLin^{DTR,3weeks}$ tendon cell number (F). N=3.Measurement of metatarsophalangeal (MTP) joint flexion angle (G), gliding resistance (H), stiffness (I), and maximum load at failure (J) of WT and $ScxLin^{DTR,3weeks}$ uninjured tendons. N=7-10 per genotype. Second harmonic generation (K) and quantification (L) of collagen fibril dispersion of WT and $ScxLin^{DTR,3weeks}$. N=3 per genotype. Nuclei stained with DAPI. Tendon is outlined by white dotted lines. Student's t-test used to assess statistical significance between genotypes. * indicates $p < 0.05$, *** indicates $p < 0.001$.

Ablation of Scx^{Lin} tendon cells significantly affected tendon homeostasis 3 months post-depletion.

To assess the requirement for Scx^{Lin} tendon cells in maintaining adult tendon homeostasis, 10-12-week-old WT and $ScxLin^{DTR}$ mice were injected with DT to induce cell death and harvested after 3 months ($ScxLin^{DTR,10weeks}$) (Fig. 8A). $ScxLin^{DTR,10weeks}$ mice had a 62.3 % decrease in tendon cell number relative to WT littermates ($p < 0.0001$)(Fig. 8B & C), demonstrating that tendon cell number had not rebounded in the three months since initial depletion (Fig. 1 E & F). Interestingly, we consistently observed a significant accumulation of unidentified cells on the top and bottom regions of $ScxLin^{DTR,10weeks}$ tendons (Fig. 8B & D). Quantification of the cellular density revealed a significant increase on the top ($p < 0.0001$) and bottom ($p < 0.01$) regions of the $ScxLin^{DTR,10\ weeks}$ compared to WT littermates (Fig. 8E). $ScxLin^{DTR,10weeks}$ tendons did not exhibit an influx of F4/80+ macrophages or tendon cell differentiation into αSMA+ myofibroblasts in either genotype (Fig. 8F). Functionally, there were no significant changes in tendon gliding function or biomechanical properties between genotypes after 3 months (Fig. 8G-J). However, second harmonic generation imaging revealed a significant increase in overall collagen fibril dispersion in $ScxLin^{DTR,10weeks}$ relative to WT littermates (WT: 8.327 degrees $\pm$ 0.39, $ScxLin^{DTR,10weeks}$: 9.815 degrees $\pm$ 0.53, p=0.0393) (Fig. 8K & L). Based on the spatial changes in cellularity (Fig. 8E), we also quantified fibril dispersion in a more spatially specific manner (top, middle and bottom thirds of the tendon) (Fig. 8-Figure Supplement 1 A-D). Interestingly, the top third of $ScxLin^{DTR,10weeks}$ tendons showed a significant increase in dispersion compared to all regions of WT (Fig. 8- Figure Supplement 1E). These data suggest a potential relationship between the increased cellularity and fibril dispersion levels on the top region of the $ScxLin^{DTR}$ FTs.

Given these changes in collagen alignment, we further assessed the ECM structure using TEM. (Fig. 8- Figure supplement 2A & B). Collagen fibril diameter distribution was substantially altered between WT (median=147.95, Q1=118.73, Q3=179.45) and $ScxLin^{DTR,10weeks}$ (median=213.41, Q1=167.49, Q3=261.91) (Fig. 8- Figure supplement 2C). Collagen fibril diameter of $ScxLin^{DTR,10weeks}$ increased by 30.67% compared to WT ($p<0.0001$) (Fig. 8- Figure supplement 2D). The collagen fibril density of $ScxLin^{DTR,10weeks}$ decreased by 48.72% compared to WT ($p<0.0001$) (Fig. 8- Figure supplement 2E). Finally, both the WT and the

$ScxLin^{DTR,10weeks}$ groups exhibited similar levels of fibril irregularity ($p = 0.9023$) (Fig. 8- Figure supplement 2F).

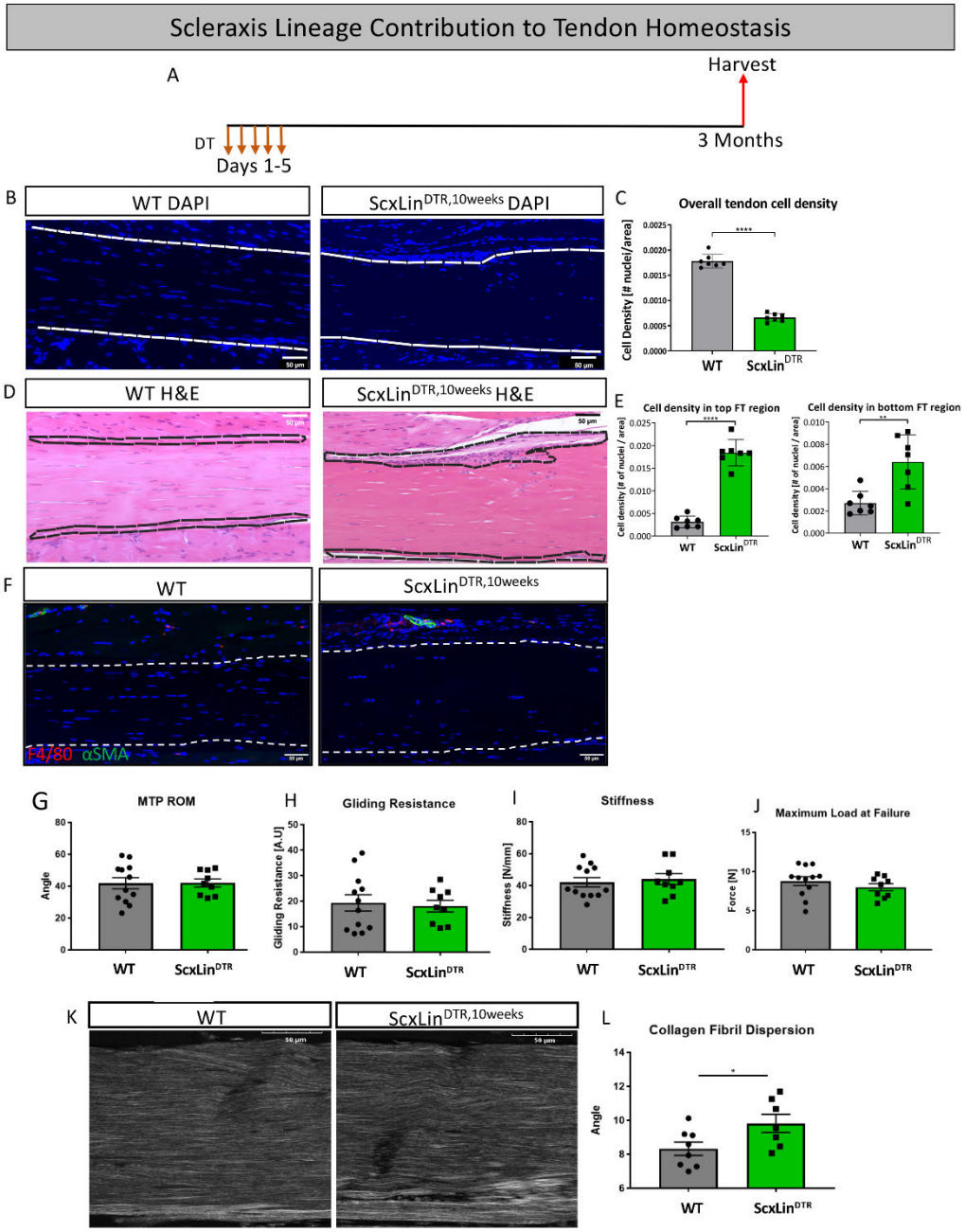

Figure 8. Tendon cell ablation negatively affected tendon homeostasis 3 months post-ablation. Mice received five hindpaw injections of DT on consecutive days at 10-12 weeks of age and were harvested uninjured 3 months later for biomechanical, gliding, and histological evaluation (ScxLin^{DTR,10weeks}) (A). Cellularity was assessed using DAPI (B) and quantified (C) 3 months after Scx^{Lin} cell depletion. H&E staining (D) was used to better define the hypercellular regions near the tendon epitenon. Cell density was quantified at the top and bottom boundaries of the tendon (E). N=7 per genotype. Co-immunofluorescence of F4/80 (macrophages) and αSMA (myofibroblasts) in uninjured WT and ScxLin^{DTR} tendons (F). N=3 per genotype. Measurement of metatarsophalangeal (MTP) joint flexion angle (G), gliding resistance (H), stiffness (I), and maximum load at failure (J) of WT and ScxLin^{DTR,10weeks} uninjured tendons. N=9-12 per genotype. Second harmonic generation (SHG) (K) and quantification (L) of collagen fibril dispersion of WT and ScxLin^{DTR,10weeks}). N=7-8 per genotype. Nuclei stained with DAPI. Tendon is outlined by white dotted lines. Student's t-test used to assess statistical significance between genotypes. * indicates $p < 0.05$.

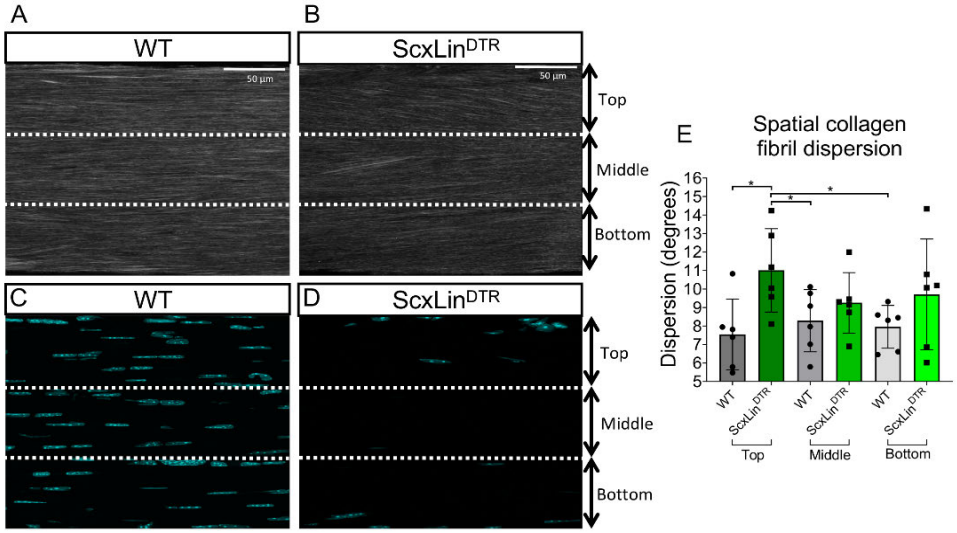

Figure 8 – Figure Supplement 1. Collagen fibrils in the top third FT region have an altered organization at 3 months post-depletion. Representative SHG images of collagen fibrils (A, B) and cell nuclei (C, D). Quantification of spatial collagen fibril dispersion on the top, middle, and bottom regions of WT and ScxLin^{DTR} FTs at 3 months post-depletion (E). N=6 per genotype. Two-way ANOVA used to assess statistical significance between genotypes and tendon regions. *indicates $p < 0.05$.

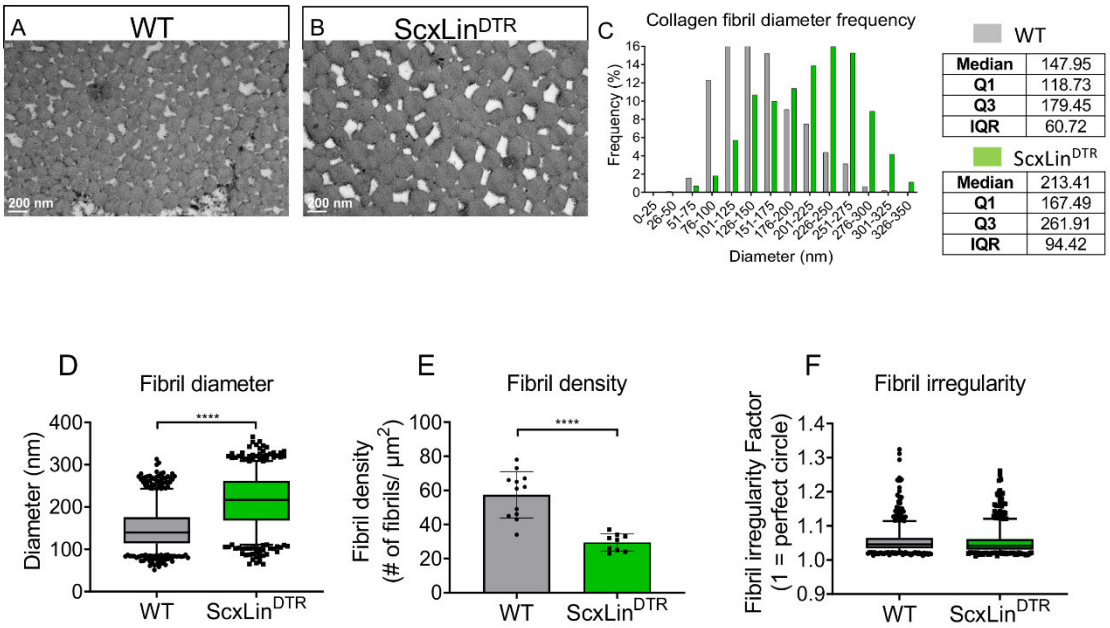

Figure 8 – Figure Supplement 2. Collagen fibrils exhibit an altered diameter and density at 3 months post-depletion. Representative TEM images of the WT and ScxLin^{DTR} FTs at 3 months post-depletion (A, B). Collagen fibril diameter histogram demonstrates an increase in the median fibril diameter in DTR D90 FTs compared to WT (C). Collagen fibril diameter of the WT and DTR D90 FTs with boxplot whiskers spanning data between the 5th and 95th percentiles; data outside this range are plotted as individual points (D). Collagen fibril density of the WT and DTR D90 FTs (E). Collagen fibril irregularity of the WT and DTR D90 FTs (F). N=4 for WT and N=3 for DTR D90. Student's t-test used to assess statistical significance between genotypes. ****indicates $p < 0.0001$.

Discussion

Previous work has established the importance of *Scx* expression in tendon development[8], growth[23], and healing[11], but few studies have considered the direct contributions of Scx^{Lin} tendon cells to these process. In the present study we examined the function of Scx^{Lin} tendon cells during adult flexor tendon healing and made the surprising discovery that Scx^{Lin} cell depletion significantly enhanced biomechanical properties by day 28 post-repair. We characterized key cell populations known to be important in healing and regeneration and utilized RNA-Seq to investigate the mechanism driving these biomechanical changes. Lastly, we examined the effects of Scx^{Lin} cell depletion on post-natal tendon growth and adult tendon homeostasis and found that Scx^{Lin} cells are required for maintenance of collagen ECM alignment and organization in adult, but not early post-natal flexor tendons.

Tendon cell depletion had surprisingly beneficial effects on healing, with biomechanical properties significantly increased at day 28 post-repair relative to WT, with no impact on gliding function. These results indicate that the improved biomechanical properties are likely not due to increased levels of disorganized matrix/scar within the healing tendon, but that the healing process may be shifted towards a regenerative phenotype. Equally striking is that the significant improvements in biomechanical properties did not emerge until 28 days post-repair, which is firmly into the remodeling phase of healing and is consistent with the low DEG number at day 14 post-repair relative to day 28. This suggests that Scx^{Lin} cells are important in the late proliferative-remodeling phases of healing and possibly enact their greatest effects by modulating the remodeling process. Our RNA-Seq results revealed significant changes in matrix-related gene expression at day 28 post-repair, suggesting that the matrix composition of the healing tendon may be substantially altered in the absence of Scx^{Lin} cells, with a shift toward either a more regenerative or mature matrix composition. Future proteomics analysis and additional experimentation will be required to further examine the matrix differences between $ScxLin^{DTR}$ and WT healing flexor tendons. It has previously been reported that tendon strength remains significantly decreased relative to uninjured controls 63 days post-repair using this flexor tendon repair model in C57Bl/6J mice[28]. Therefore, it could be beneficial to examine time points beyond day 28 to see if $ScxLin^{DTR}$

tendons reach equivalency with uninjured controls. The improved biomechanical properties contrasted with our original hypothesis which predicted that *Scx*^{Lin} cells would be necessary for proper healing and would contribute to formation of the bridging collagen tissue. Both ScxLin^{DTR} and WT mice exhibited a collagen bridge at 14- and 28-days post-repair suggesting that Scx^{Lin} cells are not the predominant cell population laying down this collagenous matrix. This is surprising due to studies demonstrating that *Scx* promotes collagen formation[11,20], highlighting the important distinction between Scx^{Lin} cells and active *Scx* expression.

While myofibroblast persistence is considered a primary driver of fibrosis[29], recent work has revealed that myofibroblasts are a highly heterogenous population with differences in pro-fibrotic markers, gene expression, and cross-linking ability, suggesting that myofibroblasts contribute to both fibrotic and regenerative processes[30]. Despite the elevated myofibroblast presence in ScxLin^{DTR} repairs at day 28, these tendons healed with increased biomechanical properties while experiencing no deficits in tendon range of motion, suggesting a regenerative rather than fibrotic healing process. Future work to comprehensively define the myofibroblast landscape in both WT and ScxLin^{DTR} mice is necessary to determine if ScxLin^{DTR} myofibroblasts are more "pro-regenerative" than those present in WT repairs. Similarly, understanding how myofibroblast subtypes affect matrix deposition at the repair site represents an important area of future study.

The RNA-seq data suggests that healing ScxLin^{DTR} tendons exhibit less overall metabolic activity compared to WT repairs at day 28. This is highlighted in IPA's canonical pathways core analysis, where "Oxidative Phosphorylation," "TCA Cycle II," "Glycolysis I," and "Gluconeogenesis I" were all predicted to be negatively enriched ("suppressed") (Fig. 6, Supplemental Table 1). Additionally, IPA's disease and function core analysis predicts an inhibitory effect on "Consumption of oxygen," while simultaneously predicting "Metabolism of carbohydrate" activation, increased "Synthesis of carbohydrate," and "Glucose metabolism disorder (Table 1)." It has previously been demonstrated in a variety of tissues that metabolic reprogramming is important for cellular differentiation and regeneration[31-34]. In addition to the dysregulation of metabolism, our RNA-seq data also revealed an increase in "Production of reactive oxygen species," "Synthesis of reactive oxygen species," and "Metabolism of reactive oxygen species (Table 1)." Despite reactive oxygen species

(ROS) being implicated in various pathologies[35], recent studies have also identified functional roles for ROS in regeneration[36-39]. While little is currently understood about the role of metabolism and ROS in tendon healing, these data clearly identify how changes in the cellular composition of the healing tendon can shift both the metabolic profile and the healing program. As such, investigating metabolic reprogramming and the dynamic roles of ROS in acute tendon healing represents an exciting area of future work.

In addition to investigating the role of tendon cells during healing, we also utilized ScxLin^{DTR} mice to assess how tendon cell ablation affected post-natal tendon growth (ScxLin^{DTR,3weeks}) and adult tendon homeostasis (ScxLin^{DTR,10weeks}). Although there were no significant differences in gliding function or biomechanical properties between ScxLin^{DTR} and WT genotypes in either age group, ScxLin^{DTR,10weeks} animals exhibited significantly increased overall collagen fibril dispersion, as well as significant changes in dispersion in specific regions of the tendon. While it is unclear what is driving these spatially-specific changes in fibril organization, it is notable that the most profound changes occur in the top epitenon region rather than endotenon, and that this area is consistent with altered and increased cellularity in ScxLin^{DTR,10weeks} tendons, though the identity and function of these cells are as yet unknown. In addition to matrix alignment, ScxLin$^{DTR,10\ weeks}$ also increased collagen fibril diameter as measured by TEM. Interestingly, one potential interpretation of the TEM data relates to the loss of proteoglycans (PGs) on the surface of the collagen fibrils, which normally prevents lateral fusion of collagen fibrils. Numerous *in vitro* and in vivo studies have shown the importance of the PGs to maintain the normal collagen fibril structure. Using proteinase treatment to remove surface bound PGs, Graham *et al*., demonstrated lateral collagen fibril aggregation, resulting in fused fibrils with increased diameter [40]. In addition, Decorin-/- tail tendons also demonstrated lateral fusion and increased fibril diameter, relative to WT [41]. While there is no direct evidence of PG production by Scx+ cells, Scx-/- hearts have decreased PG content [42,43], while Sakabe *et al*., found that Scx-/- tendons lacked fibromodulin production during tendon healing [11]. Moreover, recent work has shown that Scx knockdown in adult equine tendon cells alters the PG environment [44]. Collectively, these data suggest that the increase in fibril diameter observed in ScxLin^{DTR}, 10weeks could be due to diminution of PG production following depletion of Scx^{Lin} cells. However, we have

not directly tested this, and future proteomic studies will be required to determine if and which specific PGs may be altered following Scx^{Lin} cell depletion. Collectively, these data indicate that loss of Scx^{Lin} cells may be detrimental to tendon tissue maintenance, but that negative biomechanical effects are not yet manifested 3-months post-depletion. Future studies looking beyond the 3-month time-point will be informative to understand the role of tendon cells on maintenance of tendon tissue. It is also possible that negative effects on tendon biomechanical properties could be the result of Scx^{Lin} cell death in non-tendon tissues, such as muscle in the hindpaw[45]. Despite nearly identical depletion efficiencies between $ScxLin^{DTR,3weeks}$ and $ScxLin^{DTR,10weeks}$ animals, only $ScxLin^{DTR,10weeks}$ tendons exhibited collagen disorganization and differences in fibril size. This suggests possible differences in tendon cell sub-populations present during growth and homeostasis, as well as the potential contribution of extrinsic progenitor populations to tendon growth[13], such that depletion could differentially impact post-natal growth and adult tendon homeostasis.

We had initially planned to deplete tendon cells using the inducible $Scx\text{-}Cre^{ERT2}$ crossed to the diphtheria toxin A mouse[46], but insufficient recombination occurred and targeted cell death was not achieved. Therefore, to successfully deplete tendon cells, Scx-Cre mice were crossed to a diphtheria toxin receptor mouse model ($ScxLin^{DTR}$)[47]. The initial attempt to deplete cells using this model employed a series of intraperitoneal injections (200ng/day) and resulted in all $ScxLin^{DTR}$ mice dying within four days of the initial injection while WT animals were unaffected. $ScxLin^{DTR}$ mice likely died due to apoptosis of non-tendon/ligament associated Scx^{Lin} cells. For example, it has previously been shown that *Scx* is expressed in the lung[24,48], kidney[24], muscle[45], and brain,[48] among others. Therefore, to successfully utilize this model of cell depletion while simultaneously preventing $ScxLin^{DTR}$ associated death, a series of low-dose (20 ng/day) local hind paw injections were administered. We successfully utilized this model of *in vivo* tendon cell depletion and reached a depletion level of 57%. Therefore, the $ScxLin^{DTR}$ data should be viewed as a model of partial depletion as ~40% of tendon cells remained using this approach. Future work utilizing increased or prolonged DT treatment could be attempted to obtain more complete tendon cell depletion, and to determine if the beneficial effects of tendon cell depletion may be reversed with complete ablation of Scx^{Lin} cells from the tendon. Additionally, our current $ScxLin^{DTR}$

ablation model targets cells prior to injury and thus does not target any cells that turn on *Scx* after injury. It has previously been shown that *Scx* knockout during Achilles tendon healing drives incomplete remodeling of type III collagen to type I collagen[11]. It could be interesting to assess if depletion of cells actively expressing *Scx* during healing resulted in deleterious effects on healing. However, local DT injection into the hind paw following repair surgery represents a technical challenge as repeated injections to the healing tendon is likely to disrupt the normal healing process.

Altogether, these data demonstrate that Scx^{Lin} cell depletion is beneficial for tendon healing as it increases biomechanical properties several weeks after repair, possibly due to alterations in matrix composition, deposition, and/ or remodeling by αSMA+ myofibroblasts. Moreover, we have identified several molecular pathways that are altered following Scx^{Lin} cell depletion, such as changes in metabolism, cell motility, and the cytoskeleton, which may represent important targets for successfully modulating the healing process. Finally, Scx^{Lin} depletion does not significantly disrupt the biomechanical properties of tendons during early post-natal growth or adult tendon homeostasis within three months of Scx^{Lin} cell depletion. However, given the changes in matrix alignment and organization in adult $ScxLin^{DTR}$ tendons, it is possible that mechanical changes may occur following longer periods of depletion. Understanding the complex nature of tendon cells during healing, growth, and homeostasis can provide us with insights for driving regenerative healing and healthy tendon maintenance in the future.

Methods

Mice

Scx-Cre mice were generously provided by Dr. Ronen Schweitzer. C57Bl/6J (#000664), ROSA-Ai9$^{F/F}$ (#007909), and DTR$^{F/F}$ (#007900) mice were obtained from the Jackson Laboratory (Bar Harbor, ME, USA). ROSA-Ai9$^{F/F}$ mice express Tomato red fluorescence in the presence of Cre-mediated recombination[49]. Scx-Cre mice were crossed to ROSA-Ai9$^{F/F}$ mice to label *Scx* lineage cells (Scx^{Lin}). Diphtheria toxin receptor (DTR$^{F/F}$) mice can be utilized to temporally ablate cell populations driven by a non-inducible Cre driver[47]. In short, diphtheria toxin receptors are present on cells expressing Cre such that administration of diphtheria toxin (DT) to these mice results in targeted cell death. Scx-Cre mice were crossed to DTR$^{F/F}$ animals to generate a model of Scx^{Lin} tendon cell depletion (ScxLin^{DTR}) and Cre- wildtype littermates (WT). All mouse studies were performed with 10-12-week-old male and female mice except where otherwise noted (Figure 7, 3-4-week-old male and female mice). All mouse work (injections, surgeries, harvests) were performed in the morning. Mice were kept in a 12-hour light/dark cycle.

Flexor Tendon Repair

Complete transection and repair of the murine flexor digitorum longus (FDL) tendon was performed as previously described[50]. Mice received a 15-20µg injection of sustained-release buprenorphine. Mice were anesthetized with Ketamine (60mg/kg) and Xylazine (4mg/kg). To reduce chances of rupture at the repair site, the FDL tendon was first transected at the myotendinous junction and the skin was closed with a 5-0 suture. Next, a small incision was made to the posterior surface of the right hind paw, the FDL tendon was isolated from surrounding tissue and completely transected. The tendon was repaired using 8-0 suture and the skin was closed with a 5-0 suture. Animals resumed prior cage activity, food intake, and water consumption immediately following surgery.

Quantification of Tendon Cell Depletion and Scx^{Lin} Cells

$ScxLin^{DTR}$ mice were injected with 20ng of diphtheria toxin (DT) for five consecutive days (100ng total DT). Uninjured hind paws were harvested 10 days after the final injection for frozen sectioning. Scx^{Lin} hind paws were harvested uninjured hind paws were fixed in 10% NBF for 24 hours, decalcified in 14% EDTA for four days, and processed in 30% sucrose to cryo-protect the tissue. Samples were embedded using Cryomatrix (Thermo Fisher Scientific, Waltham, MA, USA) and sectioned into 8 mm sagittal sections using an established cryotape-transfer method[51]. Sections were stained with DAPI to visualize nuclei and imaged using a VS120 Virtual Slide Microscope (Olympus, Waltham, MA). Using Image J, a region of interest (ROI) was drawn around the tendon and an area was obtained. For $ScxLin^{DTR}$ and WT littermate mice, nuclei within the ROI were manually counted and total nuclei number was normalized to area. For Scx^{Lin} mice, fluorescent cells in uninjured sections were manually counted and Scx^{Lin+} cells reported as a percentage of total cells counted in each section. An n = 3-4 (adult mice) or n = 3-5 (young mice) was used for quantification.

Paraffin Histology and Immunofluorescence

$ScxLin^{DTR}$ hind paws were harvested 10-days after the final DT injection for homeostasis studies, and at 14- and 28-days post-repair. Additionally, uninjured $ScxLin^{DTR}$ hind paws from adult (10-12 weeks) and pre-pubescent (3-4 weeks) mice were harvested 3 months following the final DT injection to assess effects of tendon cell depletion on tendon growth and homeostasis. Hind paws were fixed in 10% neutral buffered formalin (NBF) at room temperature for 72 hours and were subsequently decalcified in Webb Jee EDTA (pH 7.2-7.4) for 7 days at room temperature, processed, and embedded in paraffin. Three-micron sagittal sections were utilized for analysis, except for the 3-month study which were cut at 5-micron to facilitate SHG imaging. $ScxLin^{DTR}$ repair sections were stained with Alcian blue/hematoxylin and Orange G (ABHOG) or Hematoxylin and eosin (H&E) to assess tissue morphology and cellularity, and Masson's Trichrome to assess collagen deposition. For immunofluorescent staining, sections were stained with Cleaved Caspase 3 (1:100, Cat#: 9661, Cell Signaling,

Danvers, MA), PCNA (1:100, Cat#:ab29, Abcam, Cambridge, MA), F4/80 (1:500, Cat#: sc-26643, Santa Cruz, Dallas, TX), α-SMA-CY3 (1:200, Cat#: C6198, Sigma Life Sciences, St. Louis, MO), α-SMA-FITC (1:500, Cat#: F3777, Sigma Life Sciences, St. Louis, MO), S100a4 (1:2000, Cat#: ab197896, Abcam, Cambridge, MA), SCXA (1:500, ab58655, Abcam, Cambridge, MA) or tdTomato (1:500, Cat#: AB8181, SICGEN, Cantanhede, Portugal). Sections were counterstained with the nuclear DAPI stain and imaged with a VS120 Virtual Slide Microscope (Olympus, Waltham, MA).

Quantification of Fluorescence

Fluorescent images scanned by the virtual slide scanner were quantified using Visiopharm image analysis software v.6.7.0.2590 (Visiopharm, Hørsholm, Denmark). Automatic segmentation via a threshold classifier was utilized to define and quantify specific cell populations based on fluorescence. An ROI was drawn to encapsulate both the scar tissue and tendon stubs. The area of fluorescent signal was determined and normalized to the total ROI area to determine percentages of each cell type. An n = 4 was used for quantification. Three samples were utilized for quantification of *Scx*+ and *S100a4*+ cells in uninjured ScxLin^{DTR} hind paws 10 days after the final DT injection. Fluorescent cells were manually counted within an ROI and normalized to either the ROI area or to both the ROI area and total cell number.

Quantitative Assessment of Gliding Function and Biomechanical Properties

Gliding function of uninjured and repaired ScxLin^{DTR} tendons was assessed as previously described[52]. Hindlimbs were harvested at the knee-joint and the FDL tendon was disconnected at the myotendinous junction. The FDL tendon was secured between two pieces of tape using superglue and the tendon was loaded incrementally with small weights ranging from 0 to 19g. Images were captured unloaded and after each load and measurements of the flexion angle of the metatarsophalangeal (MTP) joint were made using Image J. Gliding resistance was derived from the changes in MTP flexion angle over the range of applied loads. An increase in Gliding Resistance and decrease in MTP Flexion Angle is associated with restricted range of motion

and increased scar tissue. After conclusion of gliding testing, the FDL tendon was released from the tarsal tunnel while the proximal end of the tendon and the toes of the hind paw were secured into an Instron 8841 uniaxial testing system (Instron Corporation, Norwood, MA). The tendon was loaded until failure at a rate of 30mm/minute. Seven-12 samples per genotype per time-point were assessed.

RNA Extraction, Next Generation Sequencing, and Data Analysis for RNA-Seq

Tendons (three samples per genotype per time point) were harvested at 14- and 28-days post-repair and flash frozen in liquid nitrogen. Total RNA was isolated using the Bullet Blender (Next Advance) to homogenize the tissue. The RNA was isolated from the resulting extract using Trizol (Life Technologies, Carlsbad, CA) and the RNeasy Plus Micro Kit (Qiagen, Valencia, CA) per manufacturer's recommendations. The total RNA concentration was determined with the NanoDrop 1000 spectrophotometer (NanoDrop, Wilmington, DE) and RNA quality assessed with the Agilent Bioanalyzer (Agilent, Santa Clara, CA). The RNA integrity number (RIN) for all harvested samples was 8.4 $\pm$ 0.85 (mean $\pm$ standard deviation). The TruSeq Stranded mRNA Sample Preparation Kit (Illumina, San Diego, CA) was used for next generation sequencing library construction per manufacturer's protocols. Briefly, mRNA was purified from 200ng total RNA with oligo-dT magnetic beads and fragmented. First-strand cDNA synthesis was performed with random hexamer priming followed by second-strand cDNA synthesis using dUTP incorporation for strand marking. End repair and 3` adenylation was then performed on the double stranded cDNA. Illumina adaptors were ligated to both ends of the cDNA and amplified with PCR primers specific to the adaptor sequences to generate cDNA amplicons of approximately 200-500bp in size. The amplified libraries were hybridized to the Illumina flow cell and single end reads were generated for each sample using Illumina NovaSeq6000. The generated reads were demultiplexed using bcl2fastq version 2.19.0. Data cleaning and quality control was accomplished using FastP version 0.20.0. Read quantification was accomplished using subread-1.6.4 package (featureCounts). Data normalization and differential expression analysis of ScxLin^{DTR} relative to WT at a given time point was performed using DESeq2-1.22.1 with an adjusted p-value threshold of 0.05 on each set of raw expression measures. The

'lfcShrink' method was applied, which moderates log2 fold-changes for lowly expressed genes. DeSeq2 data was uploaded to Qiagen's ingenuity pathway analysis (IPA, http://www.ingenuity.com) and submitted to core analysis. Canonical pathways, upstream regulators, and downstream disease and functions were deemed biologically and statistically significant when the calculated ABS(z-score) ≥ 2 and p-value ≤ 0.05. Additionally, imposed upon the upstream regulator data was an expression log ratio cut-off of 0.5, and agreement between predicted activation state and directionality of expression log ratio. The data consists of three biological replicates per genotype per timepoint. The data generated in this study have been uploaded to the Gene Expression Omnibus under accession number GSE156157.

Second Harmonic Generation 2-Photon Confocal Imaging

Five-micron paraffin sections of WT and ScxLin^{DTR} hind paws were utilized for second harmonic generation (SHG) imaging. Sections were scanned with a Spectra-Physics MaiTai HP DeepSee Ti:Sapphire Laser, tuned to 1000nm, under 25x magnification, with a 2.5X optical zoom, with a step size of 0.25µm. 3D projections of image stacks were generated using the 3D-Project macro in ImageJ and analyzed for collagen fibril uniformity using the Directionality macro. The Directionality macro utilizes Fourier transform analysis to derive spatial orientation of image stacks. Three samples per genotype were used to quantify overall collagen fibril dispersion for pre-pubescent studies, while sections were analyzed from 7-8 mice per genotype for the adult homeostasis studies. To quantify spatial dispersion in adult samples, each image stack was divided into equal thirds (top, middle, and bottom), and dispersion was calculated within each region using Directionality macro as above. N=6 per genotype per age group were used to quantify the spatial collagen fibril dispersion.

Transmission Electron Microscopy Imaging and Analysis

FDL tendons were isolated (N = 4 for WT; N=3 for ScxLin^{DTR,10weeks}) and fixed in Glutaraldehyde Sodium Cacodylate fixative. One-micron axial sections were cut and stained with Toluidine blue. One-micron sections were then trimmed to 70 nm and stained with uranyl acetate and lead citrate. Sections were placed on grids for

imaging on a Hitachi 7650 Analytical TEM. Three non-overlapping images were taken from mid-substance of each tendon at 40,000x magnification. For measurement of fibril diameter, a region of interest (ROI) was determined within each image so that a minimum of 80 fibrils could be measured. Diameters were measured along the y-axis. The perimeter and the area of the collagen fibrils were quantified. The radii based on the calculated perimeter and area were quantified. The ratio of these two radii represent a measure of fibril roundness (fibril irregularity factor; FIF). An FIF different than 1 suggest that the fibril is not a perfect circle.

Statistical analysis and animal stratification

Experimental N determined based on previously published work[4,25]. Quantitative data was analyzed via GraphPad Prism and is presented as mean $\pm$ standard error of the mean (SEM). Either a student's t-test or two-way analysis of variance (ANOVA) with Sidak's multiple comparisons test was used to analyze data when data was normal. A Mann-Whitney test was utilized when data was not distributed normally [*Scx*+ cells normalized to area and total cell number (Figure 1, supplement 1C), D28 F4/80 and S100a4 immunofluorescence (figure 4)]. GraphPad Prism was used to detect outlier data points (ROUT method, Q-value = 1%) and no outliers were found. Mice were randomly selected for specific experimental outcome metrics prior to surgery and quantitative data (ex. fluorescence quantification, gliding and biomechanical properties) were analyzed in a blinded manner. For all experiments, an N=1 represents one mouse. p values ≤ 0.05 were considered significant. * indicates $p<0.05$, ** indicates $p<0.01$, *** indicates $p<0.001$, **** indicates $p<0.0001$.

Study Approval

This study was carried out in strict accordance with the recommendations in the Guide for the Care and Use of Laboratory Animals of the National Institutes of Health. All animal procedures described were approved by the University Committee on Animal Research (UCAR) at the University of Rochester Medical Center.

Author contributions: Study conception and design: KTB, AEL; Acquisition of data: KTB, AK, KMM, EK; Analysis and interpretation of data: KTB, AK, MRB, AEL; Drafting of manuscript: KTB, ,AK, AEL; Revision and approval of manuscript: KTB, AK, KMM, EK, MRB, AEL.

Acknowledgements: We would like to thank the Histology, Biochemistry and Molecular Imaging (HBMI) and the Biomechanics, Biomaterials and Multimodal Tissue Imaging (BBMTI) for technical assistance with the histology and biomechanical testing, respectively. We would also like to thank the URMC Multiphoton & Analytical Imaging Center (MAGIC) for assistance with Second Harmonic Generation Imaging, the UR Genomics Research Core for assistance with RNA sequencing experiment and the Electron Microscopy Core for assistance with the transmission electron microscopy data.

Funding: This work was supported in part by NIH/ NIAMS F31 AR074815 (to KTB), K01AR068386 and R01AR073169 (to AEL) and R01AR070765 (to MRB). The HBMI and BBMTI Cores were supported by NIH/ NIAMS P30AR069655. The content is solely the responsibility of the authors and does not necessarily represent the official views of the National Institutes of Health.

Competing Interests: The authors declare no competing interests.

Data Availability Statement: The RNA-Seq raw and processed data, as well as the data directly uploaded into IPA for analysis, were deposited into the Gene Expression Omnibus under accession code GSE156157.

Figure Legends

Figure 1. Model of Scleraxis lineage tendon cell depletion. Scx-Cre mice were crossed to ROSA-Ai9 reporter mice to trace (A) and quantify (B) *Scx* lineage cells (Scx^{Lin}) in uninjured flexor tendon. N=3. To deplete Scx^{Lin}, Scx-Cre mice were crossed to the diphtheria toxin receptor mouse ($ScxLin^{DTR}$, C). Mice received five hind paw injections of DT and were harvested ten days after the final injection (D). Hind paw sections from both WT and $ScxLin^{DTR}$ injected hind paws contralateral hind paws (E). Quantification of injured and contralateral hind paw tendon cell number (F). When needed, tendon outlined by white dotted line. Nuclei stained with DAPI. N=3-4 per genotype. 2-way ANOVA with Sidak's multiple comparisons test used to assess statistical significance of tendon cell ablation between hind paw (injected with DT or contralateral) and genotype (WT and $ScxLin^{DTR}$). **** indicates $p<0.0001$ relative to all other groups.

Figure 1 – Figure Supplement 1. *Scx*+ and *S100a4*+ tendon cells following Scx^{Lin} depletion. WT and $ScxLin^{DTR}$ hind paws were harvested uninjured 10 days following final DT injection and stained for either *Scx* (A-C) or *S100a4* (D-F). Quantification of *Scx*+ cells normalized to either total area (B) or both area and total cell number (C). Quantification of *S100a4*+ cells normalized to either total area (E) or both area and total cell number (F). N=3 per genotype. Statistical significance between genotypes determined using Student's t-test when data was normal (B, E, F) or Mann-Whitney test when data not normal (C). * indicative of $p \leq 0.05$.

Figure 1 – Figure Supplement 2. $ScxLin^{DTR}$ does not cause substantial effects on surrounding tissue. Assessment of apoptosis (Cleaved Caspase 3, A), proliferation (PCNA, B), and Inflammation (F4/80, macrophages, C) for WT and $ScxLin^{DTR}$ uninjured tendons. Tendon outlined by white dotted line. Nuclei stained with DAPI. Examples of positive stain indicated by yellow arrows. N=3 per genotype.

Figure 2. $ScxLin^{DTR}$ tendons heal with significantly increased biomechanical properties. Mice received five hind paw injections of DT on consecutive days, underwent flexor tendon repair surgery ten days after the

final DT injection, and were harvested at 14- and 28-days post-repair (A). Measurement of metatarsophalangeal (MTP) joint flexion angle (B), gliding resistance (C), stiffness (D), and maximum load at failure (E) of WT and ScxLin^{DTR} repaired tendons. N=9-12 per genotype per timepoint. Students t-test used to assess statistical significance between genotypes at a given timepoint. * indicative of $p < 0.05$, ** indicative of $p < 0.01$.

Figure 3. Scx^{Lin} cell depletion does not disrupt formation of a bridging collagen matrix. Mice received five hindpaw injections of DT on consecutive days, underwent flexor tendon repair surgery ten days after the final DT injection, and were harvested at 14 and 28 days post-repair (A). Alcian blue/hematoxylin and Orange G stain utilized to assess overall morphology (B). Masson's trichrome stain used to visualize collagen content and organization (C). Tendon is outlined by white dotted line and scar tissue by yellow dotted line. Black boxes indicate location of higher magnification images. Boundaries of bridging collagen indicated by black arrows. N=4 genotype per timepoint. Suture indicated by *.

Figure 4. ScxLin^{DTR} repaired tendons heal with increased presence of αSMA+ myofibroblasts. Mice received five hindpaw injections of DT on consecutive days, underwent flexor tendon repair surgery ten days after the final DT injection, and were harvested at 14 and 28 days post-repair (A). Immunofluorescence of WT and ScxLin^{DTR} repair tendons 14 and 28-days post-repair to assess F4/80+ macrophages (B), αSMA+ myofibroblasts (C), and S100a4+ cells (D). Tendon is outlined by white dotted line and scar tissue by yellow dotted line. Green boxes indicate location of higher magnification images. Examples of positive stain indicated by white arrows, while examples of auto-fluorescent blood cells and α-SMA+ blood vessels indicated by green arrows. Quantification of F4/80 (A' & A''), αSMA (B' & B''), and S100a4 (C' & C'') fluorescence. N=4 per genotype per timepoint. Student's t-test used to assess statistical significance between genotypes at a given timepoint, except for D28 F4/80 and S100a4 which required a Mann-Whitney test. * indicates $p < 0.05$.

Figure 5. Bulk RNA sequencing reveals differences between ScxLin^{DTR} and wildtype healing flexor tendons at 14 and 28 days post-repair. Representation of differentially expressed genes (DEGs) at 14 (A, B) and 28 (C, D) days post-repair. Volcano plots (A, C) depict significantly upregulated DEGs as red dots and significantly downregulated DEGs as green dots. DEGs are consider significant when the multiple test corrected (adjusted) p-value is ≤ 0.05. The dotted line represents the unadjusted p-value of 0.05. Heat maps (B, D) depict all significant DEGs, with the data representing the regularized log transformation of the normalized count data.

Figure 6. Canonical Pathways positively and negatively enriched in ScxLin^{DTR} healing tendons at day 28 post-repair. Ingenuity pathway analysis was utilized to determine positively and negatively significantly enriched pathways in ScxLin^{DTR} healing tendons at day 28 post-repair. Canonical pathways were considered significant if $p \leq 0.05$ and ABS(Z-score) ≥ 2. The orange color indicates pathways that are significantly, positively enriched ("activated"), while the blue color indicates significantly, negatively enriched ("inhibited") pathways. The orange dotted line represents -log (1.3) = 0.05, indicating the p-value cut-off.

Figure 7. Tendon cell ablation does not negatively affect post-natal tendon growth 3 months post-ablation. Pre-pubescent mice (3-4 weeks old) received five hindpaw injections of DT and were harvested ten days after the final injection to assess tendon cell depletion (ScxLin^{DTR}) (A). Hindpaw sections from both WT and ScxLin^{DTR} hindpaws (B). Quantification of WT and ScxLin^{DTR,3weeks} tendon cell number in pre-pubescent mice (C). To assess effects of tendon cell depletion on post-natal tendon growth, mice received five hindpaw injections of DT on consecutive days at 3-4 weeks of age and were harvested uninjured 3 months later for biomechanical, gliding, and histological evaluation (ScxLin^{DTR,3weeks}) (D). Co-immunofluorescence of F4/80 (macrophages) and αSMA (myofibroblasts) in uninjured WT and ScxLin^{DTR,3weeks} tendons (E). Quantification of WT and ScxLin^{DTR,3weeks} tendon cell number (F). Measurement of metatarsophalangeal (MTP) joint flexion angle (G), gliding resistance (H), stiffness (I), and maximum load at failure (J) of WT and ScxLin^{DTR,3weeks} uninjured tendons. N=7-10 per genotype. Second harmonic generation (K) and quantification (L) of collagen

fibril dispersion of WT and ScxLin^{DTR,3weeks}. N=3 per genotype. Nuclei stained with DAPI. Tendon is outlined by white dotted lines. Student's t-test used to assess statistical significance between genotypes. * indicates $p < 0.05$, *** indicates $p < 0.001$.

Figure 8. Tendon cell ablation negatively affected tendon homeostasis 3 months post-ablation. Mice received five hindpaw injections of DT on consecutive days at 10-12 weeks of age and were harvested uninjured 3 months later for biomechanical, gliding, and histological evaluation (ScxLin^{DTR,10weeks}) (A). Cellularity was assessed using DAPI (B) and quantified (C) 3 months after Scx^{Lin} cell depletion. H&E staining (D) was used to better define the hypercellular regions near the tendon epitenon. Cell density was quantified at the top and bottom boundaries of the tendon (E). N=7 per genotype. Co-immunofluorescence of F4/80 (macrophages) and αSMA (myofibroblasts) in uninjured WT and ScxLin^{DTR} tendons (F). N=3 per genotype. Measurement of metatarsophalangeal (MTP) joint flexion angle (G), gliding resistance (H), stiffness (I), and maximum load at failure (J) of WT and ScxLin^{DTR,10weeks} uninjured tendons. N=9-12 per genotype. Second harmonic generation (SHG) (K) and quantification (L) of collagen fibril dispersion of WT and ScxLin^{DTR,10weeks}). N=7-8 per genotype. Nuclei stained with DAPI. Tendon is outlined by white dotted lines. Student's t-test used to assess statistical significance between genotypes. * indicates $p < 0.05$.

Figure 8 – Figure Supplement 1. Collagen fibrils in the top third FT region have an altered organization at 3 months post-depletion. Representative SHG images of collagen fibrils (A, B) and cell nuclei (C, D). Quantification of spatial collagen fibril dispersion on the top, middle, and bottom regions of WT and ScxLin^{DTR} FTs at 3 months post-depletion (E). N=6 per genotype. Two-way ANOVA used to assess statistical significance between genotypes and tendon regions. *indicates $p < 0.05$.

Figure 8 – Figure Supplement 2. Collagen fibrils exhibit an altered diameter and density at 3 months post-depletion. Representative TEM images of the WT and ScxLin^{DTR} FTs at 3 months post-depletion (A, B).

Collagen fibril diameter histogram demonstrates an increase in the median fibril diameter in DTR D90 FTs compared to WT (C). Collagen fibril diameter of the WT and DTR D90 FTs with boxplot whiskers spanning data between the 5th and 95th percentiles; data outside this range are plotted as individual points (D). Collagen fibril density of the WT and DTR D90 FTs (E). Collagen fibril irregularity of the WT and DTR D90 FTs (F). N=4 for WT and N=3 for DTR D90. Student's t-test used to assess statistical significance between genotypes. ****indicates $p < 0.0001$.

Tables

Table 1. Ingenuity pathway analysis downstream effects - Disease and Functions. Table of all disease and function annotations marked as significant ($p \leq 0.05$ and ABS(Z-score) > 2) using IPA core analysis for $ScxLin^{DTR}$ vs WT at day 28 post-repair.

Table 2. Regulation of matrix components in $ScxLin^{DTR}$ healing tendons at day 28. Expression level, fold change, and adjusted p-value of key matrix-related genes in $ScxLin^{DTR}$ tendons vs WT at day 28 post-repair generated from bulk RNA-seq. Orange color indicative of increased expression and blue color indicative of decreased expression.

Table 3. Ingenuity pathway analysis upstream regulators. All possible upstream regulators where expression log ratio ≥ 0.5, ABS(Z-score) > 2, p-value ≤ 0.05, and agreement between predicted activation state and directionality of regulator's gene expression, compiled using IPA core analysis for $ScxLin^{DTR}$ vs WT at day 28 post-repair.

Supplemental Table 1. Ingenuity pathway analysis canonical pathways. All enriched pathways marked as significant (-log(p-value) > 1.3 and ABS(Z-score) ≥ 2) using IPA core analysis for $ScxLin^{DTR}$ vs WT at day 28 post-repair.

	Disease or Function Annotation	p-value	Activation State	Z-Score
Down-Regulated	Contractility of skeletal muscle	4.96E-16	Decreased	-3.595
	Abnormal bone density	0.000000572	Decreased	-3.299
	Contractility of muscle	8.91E-16	Decreased	-2.636
	Intestinal cancer	6.76E-46	Decreased	-2.561
	Bleeding	0.00000075	Decreased	-2.424
	Malignant neoplasm of large intestine	8.42E-46	Decreased	-2.343
	Colorectal cancer	6.67E-23	Decreased	-2.343
	Large intestine neoplasm	2.97E-46	Decreased	-2.256
	Colorectal tumor	1.28E-23	Decreased	-2.256
	Function of muscle	6.93E-14	Decreased	-2.245
	Consumption of oxygen	0.000000942	Decreased	-2.237
	Function of skeletal muscle	1.59E-08	Decreased	-2.186
	Intestinal tumor	9.72E-47	Decreased	-2.144
	Development of lung carcinoma	0.000000663	Decreased	-2.012
Up-regulated	Cell movement	4.98E-22	Increased	4.735
	Migration of cells	6.44E-17	Increased	4.733
	Cell movement of tumor cell lines	8.66E-10	Increased	4.343
	Reorganization of cytoskeleton	0.000000218	Increased	4.296
	Migration of tumor cell lines	0.00000032	Increased	4.162
	Engulfment of cells	1.05E-09	Increased	4.057
	Endocytosis	1.2E-11	Increased	3.821
	Leukocyte migration	4.37E-09	Increased	3.821
	Cell movement of blood cells	4.04E-09	Increased	3.818
	Homing of cells	0.00000055	Increased	3.792
	Formation of cellular protrusions	1.53E-14	Increased	3.669
	Glucose metabolism disorder	5.46E-10	Increased	3.516
	Invasion of cells	9.21E-08	Increased	3.396
	Organization of cytoplasm	3.25E-26	Increased	3.384
	Organization of cytoskeleton	2.94E-20	Increased	3.384
	Cell movement of leukocytes	7.74E-08	Increased	3.38
	Endocytosis by eukaryotic cells	1.16E-08	Increased	3.371
	Engulfment of tumor cell lines	0.00000031	Increased	3.348
	Proliferation of neuronal cells	3.67E-09	Increased	3.313
	Metabolism of carbohydrate	1.94E-13	Increased	3.285
	Formation of lamellipodia	0.000000932	Increased	3.121
	Cell movement of breast cancer cell lines	0.000000603	Increased	3.103
	Cell movement of fibroblast cell lines	3.42E-08	Increased	3.083
	Growth of neurites	6.25E-09	Increased	2.981
	Microtubule dynamics	5.21E-18	Increased	2.974
	Cell spreading	3.31E-11	Increased	2.875
	Formation of filopodia	0.000000177	Increased	2.873
	Cell movement of connective tissue cells	0.000000415	Increased	2.792
	Concentration of lipid	3.14E-08	Increased	2.779
	Progressive neurological disorder	6.74E-10	Increased	2.671
	Outgrowth of neurites	7.31E-08	Increased	2.662
	Production of reactive oxygen species	6.22E-12	Increased	2.625
	Quantity of macropinosomes	0.000000865	Increased	2.621
	Neuromuscular disease	1.47E-15	Increased	2.619
	Progressive myopathy	1.28E-11	Increased	2.611

Synthesis of carbohydrate	0.000000499	Increased	2.553
Outgrowth of cells	0.000000025	Increased	2.52
Advanced malignant tumor	0.000000208	Increased	2.517
Differentiation of connective tissue cells	1.48E-09	Increased	2.512
Secondary tumor	0.000000643	Increased	2.461
Arrhythmia	2.14E-08	Increased	2.4
Fibrosis	0.000000337	Increased	2.397
Extension of cellular protrusions	0.00000098	Increased	2.371
Invasive tumor	2.47E-08	Increased	2.345
Synthesis of reactive oxygen species	3.6E-14	Increased	2.312
Organization of actin cytoskeleton	4.37E-08	Increased	2.298
Disassembly of filaments	0.000000544	Increased	2.27
Metabolism of reactive oxygen species	2.61E-15	Increased	2.269
Cancer of cells	9.31E-14	Increased	2.254
Response of tumor cell lines	2.31E-08	Increased	2.231
Morphogenesis of neurons	1.44E-12	Increased	2.224
Neuritogenesis	1.86E-12	Increased	2.224
Neoplasia of cells	1.76E-16	Increased	2.221
Quantity of metal	0.0000002	Increased	2.198
Ruffling	0.000000297	Increased	2.157
Tubulation of cells	0.00000126	Increased	2.132
Angiogenesis	4.02E-15	Increased	2.109
Hereditary myopathy	1.58E-23	Increased	2.104
Dystrophy of muscle	1.85E-11	Increased	2.104
Development of vasculature	2.67E-16	Increased	2.06
Growth of axons	0.000000724	Increased	2.017
Migration of fibroblast cell lines	0.000000461	Increased	2.002

Table 1. Ingenuity pathway analysis downstream effects - Disease and Functions. Table of all disease and function annotations marked as significant ($p \leq 0.05$ and ABS(Z-score) > 2) using IPA core analysis for $ScxLin^{DTR}$ vs WT at day 28 post-repair.

Gene	BaseMean	Fold Change (Log_2)	p-adj
		Collagens	
Col1a1	742982.883	0.275	0.117206
Col1a2	720257.233	0.359	0.033355
Col2a1	461.965	0.176	0.700754
Col3a1	748380.28	0.645	0.005567
Col4a1	35181.773	0.17	0.559295
Col4a2	31627.065	0.265	0.206116
Col4a3	49.144	-0.009	0.988635
Col4a4	143.52	0.232	0.589161
Col4a5	284.059	0.372	0.440755
Col4a6	52.693	-0.093	0.904823
Col5a1	118821.857	0.495	0.031814
Col5a2	105087.042	0.46	0.092164
Col5a3	35303.666	0.418	0.06355
Col6a1	122410.423	0.406	0.00366
Col6a2	122396.322	0.455	0.003183
Col6a3	55660.629	0.545	0.021485
Col6a4	33.599	-0.879	0.0385
Col6a5	72.046	0.599	0.286724
Col6a6	51.234	-0.07	0.901424
Col7a1	2215.503	-0.532	0.06829
Col8a1	6553.562	0.983	0.025451
Col8a2	4787.689	-0.128	0.727708
Col9a1	390.971	-1.328	0.000857
Col9a2	50.18	-0.071	0.911757
Col9a3	52.911	0.177	0.713852
Col10a1	4.585	0.254	N/A*
Col11a1	13080.117	-0.239	0.496276
Col11a2	1974.589	-0.671	0.028981

Col12a1	34791.768	-0.204	0.545342
Col13a1	308.833	-0.085	0.853468
Col14a1	7279.653	0.693	0.00124
Col15a1	8889.517	0.385	0.296359
Col16a1	24279.347	0.237	0.252556
Col17a1	269.42	0.002	N/A*
Col18a1	14754.886	0.391	0.169961
Col19a1	4.738	0.133	N/A*
Col20a1	438.526	-0.7	0.060808
Col22a1	2064	-0.797	0.022217
Col23a1	4457.185	-0.636	0.025351
Col24a1	966.961	-0.35	0.047102
Col25a1	118.033	0.022	0.975523
Col26a1	78.9	0.371	0.475453
Col27a1	4062.784	0.406	0.253217
Col28a1	579.441	0.291	0.653743
ECM Proteoglycans			
Hspg2	47213.867	0.248	0.108795
Aspn	19143.191	0.839	0.007556
Bgn	151131.153	0.251	0.256881
Dcn	95817.718	0.654	1.26E-05
Fmod	132295.748	0.172	0.683103
Kera	5207.231	0.522	0.154489
Lum	43114.099	0.353	0.130133
Omd	65.324	0.56	0.151367
Prelp	18853.124	0.381	0.057946
Epyc	133.935	1.187	0.003793
Ogn	5228.656	0.636	0.004079
Optc	30.193	0.042	0.957221
Chad	2558.426	-0.133	0.813626

Chadl	146.381	0.377	0.295306
Nyx	21.048	0.443	0.360179
Podn	1763.369	0.432	0.131578
Podnl1	216.612	-0.087	0.872241
Acan	8738.435	-0.407	0.194754
Bcan	125.867	-0.764	0.014902
Ncan	1.472	-0.047	N/A*
Vcan	5214.463	0.431	0.165678
Hapln1	109.201	0.036	0.955062
Hapln2	8.84	-0.024	N/A*
Hapln3	31.92	0.039	0.949531
Hapln4	128.699	0.053	0.926101
Prg2	2.717	-0.083	N/A*
Spock1	12.387	0.674	N/A*
Spock2	621.489	0.027	0.956371
Spock3	34.16	-0.034	0.963822
Prg4	26463.024	-0.191	0.759532
Srgn	1500.611	-0.08	0.843956
Impg2	49.211	-0.196	0.676547
Esm1	120.466	-0.02	0.971642
Basement Membrane Components			
Lama1	3.29	-0.445	N/A*
Lama2	3430.887	0.361	0.201711
Lama3	104.957	-0.303	0.484039
Lama4	7706.819	0.34	0.081572
Lama5	3390.382	-0.237	0.430648
Lamb1	11272.507	0.236	0.389409
Lamb2	13730.5	0.343	0.092701
Lamb3	77.394	-0.06	0.924993
Lamc1	15292.13	0.313	0.119095

Lamc2	424.266	0.393	0.064032
Lamc3	21.597	0.093	0.886633
Nid1	12717.306	0.539	0.02301
Nid2	2799.817	0.179	0.586124
Colq	358.747	-0.379	0.341156
Major ECM Glycoproteins			
Eln	17607.464	0.518	0.270402
Emilin1	6960.539	0.124	0.684821
Emilin2	4405.463	0.512	0.061758
Emilin3	595.356	0.857	0.005562
Emid1	550.685	0.252	0.631487
Fbln1	2214.023	0.23	0.320082
Fbln2	48333.486	0.127	0.615495
Fbln5	2725.675	0.326	0.023116
Fbln7	4562.409	0.784	0.00233
Efemp1	1308.939	0.543	0.077648
Efemp2	4858.991	0.222	0.11327
Fbn1	36959.196	0.668	0.005087
Fbn2	2856.248	-0.008	0.983466
Fn1	510510.053	0.307	0.223595
Fras1	430.729	-0.837	0.013797
Gldn	464.82	0.424	0.390168
Hmcn1	1034.806	0.589	0.036404
Hmcn2	6034.922	0.252	0.456036
Ibsp	2.365	-0.125	N/A*
Matn1	0.671	0.074	N/A*
Matn2	6213.381	0.503	0.015668
Matn3	201.369	-0.581	0.155595
Matn4	2796.498	-0.245	0.6134
Mfap1a	536.887	0.101	0.639732

Mfap1b	398.958	0.03	0.902813
Mfap2	3608.727	0.465	0.013072
Mfap3	1213.924	0.119	0.519005
Mfap4	4217.93	0.4	0.210242
Mfap5	14548.008	0.753	5.34E-05
Mmrn1	439.183	0.492	0.262418
Mmrn2	1557.776	-0.201	0.519886
Npnt	1084.388	-0.453	0.209896
Papln	16.561	-0.122	0.859483
Postn	102294.871	0.591	0.048873
Sparc	331616.177	0.479	0.000296
Sparcl1	12872.967	-0.027	0.959288
Spp1	29368.724	0.234	0.637831
Srpx2	5778.794	0.362	0.077229
Tnc	28609.297	0.378	0.326135
Tnn	5098.501	-0.623	0.126873
Tnr	19.271	0.482	0.385953
Tnxa	6.323	0.944	N/A*
Tnxb	18888.425	0.781	0.015263
Thbs1	14477.798	0.49	0.099587
Thbs2	36613.787	0.39	0.149809
Thbs3	17595.855	0.267	0.193149
Thbs4	203095.542	0.841	5.69E-05
Comp	35501.759	0.293	0.10314

Table 2. Regulation of matrix components in ScxLin^{DTR} healing tendons at day 28. Expression level, fold change, and adjusted p-value of key matrix-related genes in ScxLin^{DTR} tendons vs WT at day 28 post-repair generated from bulk RNA-seq. Orange color indicative of increased expression and blue color indicative of decreased expression.

Upstream Regulator	Expression Log Ratio	Predicted Activation State	Activation Z-Score	P-value of overlap
		Activated in ScxLin^{DTR}		
S100A4	0.518	Activated	2.946	0.00456
F2	0.533	Activated	2.606	0.000134
BTNL2	0.805	Activated	2.324	0.012
EBF2	0.657	Activated	2.223	0.000738
F2R	0.599	Activated	2.22	0.0243
NTRK2	0.608	Activated	2.137	0.012
SOX2	1.138	Activated	2.071	0.0000143
FGF2	0.544	Activated	2.017	0.000393
		Inhibited in ScxLin^{DTR}		
FOXO4	-0.501	Inhibited	-2.697	0.0236
MEF2C	-0.905	Inhibited	-2.577	3.06E-08
SMYD1	-0.836	Inhibited	-2.219	2.63E-12
LDHB	-0.609	Inhibited	-2.219	0.000241

Table 3. Ingenuity pathway analysis upstream regulators. All possible upstream regulators where expression log ratio ≥ 0.5, ABS(Z-score) > 2, p-value ≤ 0.05, and agreement between predicted activation state and directionality of regulator's gene expression, compiled using IPA core analysis for ScxLin^{DTR} vs WT at day 28 post-repair.

	Canonical Pathway	-log(p)	Z-Score
Negatively-Enriched			
	Oxidative Phosphorylation	7.6	-5.303
	TCA Cycle II (Eukaryotic)	5.96	-3.464
	White Adipose Tissue Browning Pathway	3.23	-2.353
	Calcium Signaling	5.72	-2.335
	Glycolysis I	4.63	-2.111
	Gluconeogenesis I	4.63	-2.111
Positively-Enriched			
	Ephrin Receptor Signaling	6.13	3.888
	Rac Signaling	3.85	3.674
	Actin Nucleation by ARP-WASP Complex	5.16	3.441
	Fcγ Receptor-mediated Phagocytosis in Macrophages and Monocytes	3.77	3.411
	Remodeling of Epithelial Adherens Junctions	6.23	3.162
	Regulation of Actin-based Motility by Rho	5.75	3.128
	Sphingosine-1-phosphate Signaling	3.94	2.711
	Ephrin B Signaling	3.09	2.53
	RhoA Signaling	3.97	2.502
	Glioma Invasiveness Signaling	2.13	2.496
	fMLP Signaling in Neutrophils	4.44	2.449
	Actin Cytoskeleton Signaling	7.86	2.214
	Production of Nitric Oxide and Reactive Oxygen Species in Macrophages	2.01	2.117

Supplemental Table 1. Ingenuity pathway analysis canonical pathways. All enriched pathways marked as significant (-log(p-value) > 1.3 and ABS(Z-score) $\geq$ 2) using IPA core analysis for ScxLin^{DTR} vs WT at day 28 post-repair.

References

1 Nichols, A. E. C., Best, K. T. & Loiselle, A. E. The cellular basis of fibrotic tendon healing: challenges and opportunities. *Translational research : the journal of laboratory and clinical medicine* **209**, 156-168, doi:10.1016/j.trsl.2019.02.002 (2019).

2 Walia, B. & Huang, A. H. Tendon stem progenitor cells: Understanding the biology to inform therapeutic strategies for tendon repair. *Journal of orthopaedic research : official publication of the Orthopaedic Research Society* **37**, 1270-1280, doi:10.1002/jor.24156 (2019).

3 Costa-Almeida, R., Calejo, I. & Gomes, M. E. Mesenchymal Stem Cells Empowering Tendon Regenerative Therapies. *International journal of molecular sciences* **20**, doi:10.3390/ijms20123002 (2019).

4 Best, K. T. & Loiselle, A. E. Scleraxis lineage cells contribute to organized bridging tissue during tendon healing and identify a subpopulation of resident tendon cells. *FASEB journal : official publication of the Federation of American Societies for Experimental Biology*, fj201900130RR, doi:10.1096/fj.201900130RR (2019).

5 Swanson, J. B. *et al.* A single-cell transcriptional atlas identifies extensive heterogeneity in the cellular composition of tendons. *bioRxiv*, 801266, doi:10.1101/801266 (2019).

6 Kendal, A. *et al.* Identification of human tendon cell populations in healthy and diseased tissue using combined single cell transcriptomics and proteomics. *bioRxiv*, 2019.2012.2009.869933, doi:10.1101/2019.12.09.869933 (2019).

7 Schweitzer, R. *et al.* Analysis of the tendon cell fate using Scleraxis, a specific marker for tendons and ligaments. *Development (Cambridge, England)* **128**, 3855-3866 (2001).

8 Murchison, N. D. *et al.* Regulation of tendon differentiation by scleraxis distinguishes force-transmitting tendons from muscle-anchoring tendons. *Development (Cambridge, England)* **134**, 2697-2708, doi:10.1242/dev.001933 (2007).

9 Pryce, B. A. *et al.* Recruitment and maintenance of tendon progenitors by TGFbeta signaling are essential for tendon formation. *Development (Cambridge, England)* **136**, 1351-1361, doi:10.1242/dev.027342 (2009).

10 Huang, A. H. *et al.* Requirement for scleraxis in the recruitment of mesenchymal progenitors during embryonic tendon elongation. *Development (Cambridge, England)* **146**, doi:10.1242/dev.182782 (2019).

11 Sakabe, T. *et al.* Transcription factor scleraxis vitally contributes to progenitor lineage direction in wound healing of adult tendon in mice. *The Journal of biological chemistry* **293**, 5766-5780, doi:10.1074/jbc.RA118.001987 (2018).

12 Howell, K. *et al.* Novel Model of Tendon Regeneration Reveals Distinct Cell Mechanisms Underlying Regenerative and Fibrotic Tendon Healing. *Scientific reports* **7**, 45238, doi:10.1038/srep45238 (2017).

13 Dyment, N. A. *et al.* Lineage tracing of resident tendon progenitor cells during growth and natural healing. *PloS one* **9**, e96113, doi:10.1371/journal.pone.0096113 (2014).

14 Bavin, E. P., Atkinson, F., Barsby, T. & Guest, D. J. Scleraxis Is Essential for Tendon Differentiation by Equine Embryonic Stem Cells and in Equine Fetal Tenocytes. *Stem cells and development*, doi:10.1089/scd.2016.0279 (2017).

15 Chen, X. *et al.* Force and scleraxis synergistically promote the commitment of human ES cells derived MSCs to tenocytes. *Scientific reports* **2**, 977, doi:10.1038/srep00977 (2012).

16 Alberton, P. *et al.* Conversion of human bone marrow-derived mesenchymal stem cells into tendon progenitor cells by ectopic expression of scleraxis. *Stem cells and development* **21**, 846-858, doi:10.1089/scd.2011.0150 (2012).

17 Nichols, A. C., Werre, S. R. & Dahlgren, L. A. Transient scleraxis overexpression combined with cyclic strain enhances ligamentous differentiation. *Tissue engineering. Part A*, doi:10.1089/ten.TEA.2017.0481 (2018).

18 Maeda, T. *et al.* Conversion of mechanical force into TGF-beta-mediated biochemical signals. *Current biology : CB* **21**, 933-941, doi:10.1016/j.cub.2011.04.007 (2011).

19 Nichols, A. E. C., Settlage, R. E., Werre, S. R. & Dahlgren, L. A. Novel roles for scleraxis in regulating adult tenocyte function. *BMC cell biology* **19**, 14, doi:10.1186/s12860-018-0166-z (2018).

20 Lejard, V. *et al.* Scleraxis and NFATc regulate the expression of the pro-alpha1(I) collagen gene in tendon fibroblasts. *The Journal of biological chemistry* **282**, 17665-17675, doi:10.1074/jbc.M610113200 (2007).

21 Levay, A. K. *et al.* Scleraxis is required for cell lineage differentiation and extracellular matrix remodeling during murine heart valve formation in vivo. *Circulation research* **103**, 948-956, doi:10.1161/circresaha.108.177238 (2008).
22 Al-Hattab, D. S. *et al.* Scleraxis regulates Twist1 and Snai1 expression in epithelial-to-mesenchymal transition. *American journal of physiology. Heart and circulatory physiology*, doi:10.1152/ajpheart.00092.2018 (2018).
23 Gumucio, J. P., Schonk, M. M., Kharaz, Y. A., Comerford, E. & Mendias, C. L. Scleraxis is required for the growth of adult tendons in response to mechanical loading. *JCI insight* **5**, doi:10.1172/jci.insight.138295 (2020).
24 Pryce, B. A., Brent, A. E., Murchison, N. D., Tabin, C. J. & Schweitzer, R. Generation of transgenic tendon reporters, ScxGFP and ScxAP, using regulatory elements of the scleraxis gene. *Developmental dynamics : an official publication of the American Association of Anatomists* **236**, 1677-1682, doi:10.1002/dvdy.21179 (2007).
25 Best, K. T., Lee, F. K., Knapp, E., Awad, H. A. & Loiselle, A. E. Deletion of NFKB1 enhances canonical NF-κB signaling and increases macrophage and myofibroblast content during tendon healing. *Scientific reports* **9**, 10926, doi:10.1038/s41598-019-47461-5 (2019).
26 Ackerman, J. E. *et al.* Cell non-autonomous functions of S100a4 drive fibrotic tendon healing. *Elife* **8**, doi:10.7554/eLife.45342 (2019).
27 Hynes, R. O. & Naba, A. Overview of the matrisome--an inventory of extracellular matrix constituents and functions. *Cold Spring Harbor perspectives in biology* **4**, a004903, doi:10.1101/cshperspect.a004903 (2012).
28 Loiselle, A. E. *et al.* Remodeling of murine intrasynovial tendon adhesions following injury: MMP and neotendon gene expression. *Journal of orthopaedic research : official publication of the Orthopaedic Research Society* **27**, 833-840, doi:10.1002/jor.20769 (2009).
29 Hinz, B. & Lagares, D. Evasion of apoptosis by myofibroblasts: a hallmark of fibrotic diseases. *Nature reviews. Rheumatology* **16**, 11-31, doi:10.1038/s41584-019-0324-5 (2020).
30 Shook, B. A. *et al.* Myofibroblast proliferation and heterogeneity are supported by macrophages during skin repair. *Science (New York, N.Y.)* **362**, doi:10.1126/science.aar2971 (2018).
31 Chen, F. *et al.* YY1 regulates skeletal muscle regeneration through controlling metabolic reprogramming of satellite cells. *The EMBO journal* **38**, doi:10.15252/embj.201899727 (2019).
32 De Santa, F., Vitiello, L., Torcinaro, A. & Ferraro, E. The Role of Metabolic Remodeling in Macrophage Polarization and Its Effect on Skeletal Muscle Regeneration. *Antioxidants & redox signaling* **30**, 1553-1598, doi:10.1089/ars.2017.7420 (2019).
33 Osuma, E. A., Riggs, D. W., Gibb, A. A. & Hill, B. G. High throughput measurement of metabolism in planarians reveals activation of glycolysis during regeneration. *Regeneration (Oxford, England)* **5**, 78-86, doi:10.1002/reg2.95 (2018).
34 Lai, L., Reineke, E., Hamilton, D. J. & Cooke, J. P. Glycolytic Switch Is Required for Transdifferentiation to Endothelial Lineage. *Circulation* **139**, 119-133, doi:10.1161/circulationaha.118.035741 (2019).
35 Schieber, M. & Chandel, N. S. ROS function in redox signaling and oxidative stress. *Current biology : CB* **24**, R453-462, doi:10.1016/j.cub.2014.03.034 (2014).
36 Santabárbara-Ruiz, P. *et al.* Ask1 and Akt act synergistically to promote ROS-dependent regeneration in Drosophila. *PLoS genetics* **15**, e1007926, doi:10.1371/journal.pgen.1007926 (2019).
37 Youm, T. H., Woo, S. H., Kwon, E. S. & Park, S. S. NADPH Oxidase 4 Contributes to Myoblast Fusion and Skeletal Muscle Regeneration. *Oxidative medicine and cellular longevity* **2019**, 3585390, doi:10.1155/2019/3585390 (2019).
38 Labit, E. *et al.* Opioids prevent regeneration in adult mammals through inhibition of ROS production. *Scientific reports* **8**, 12170, doi:10.1038/s41598-018-29594-1 (2018).
39 Santabárbara-Ruiz, P. *et al.* ROS-Induced JNK and p38 Signaling Is Required for Unpaired Cytokine Activation during Drosophila Regeneration. *PLoS genetics* **11**, e1005595, doi:10.1371/journal.pgen.1005595 (2015).
40 Graham, H. K., Holmes, D. F., Watson, R. B. & Kadler, K. E. Identification of collagen fibril fusion during vertebrate tendon morphogenesis. The process relies on unipolar fibrils and is regulated by collagen-proteoglycan interaction. *J Mol Biol* **295**, 891-902, doi:10.1006/jmbi.1999.3384 (2000).
41 Danielson, K. G. *et al.* Targeted disruption of decorin leads to abnormal collagen fibril morphology and skin fragility. *J Cell Biol* **136**, 729-743, doi:10.1083/jcb.136.3.729 (1997).

42 Barnette, D. N. *et al.* Tgfbeta-Smad and MAPK signaling mediate scleraxis and proteoglycan expression in heart valves. *J Mol Cell Cardiol* **65**, 137-146, doi:10.1016/j.yjmcc.2013.10.007 (2013).
43 Barnette, D. N., VandeKopple, M., Wu, Y., Willoughby, D. A. & Lincoln, J. RNA-seq analysis to identify novel roles of scleraxis during embryonic mouse heart valve remodeling. *PloS one* **9**, e101425, doi:10.1371/journal.pone.0101425 (2014).
44 Paterson, Y. Z. *et al.* The transcription factor scleraxis differentially regulates gene expression in tenocytes isolated at different developmental stages. *Mechanisms of Development* **Available online 11 August 2020**, doi:https://doi.org/10.1016/j.mod.2020.103635 (2020).
45 Mendias, C. L. *et al.* Transforming growth factor-beta induces skeletal muscle atrophy and fibrosis through the induction of atrogin-1 and scleraxis. *Muscle & nerve* **45**, 55-59, doi:10.1002/mus.22232 (2012).
46 Voehringer, D., Liang, H. E. & Locksley, R. M. Homeostasis and effector function of lymphopenia-induced "memory-like" T cells in constitutively T cell-depleted mice. *Journal of immunology (Baltimore, Md. : 1950)* **180**, 4742-4753 (2008).
47 Buch, T. *et al.* A Cre-inducible diphtheria toxin receptor mediates cell lineage ablation after toxin administration. *Nature methods* **2**, 419-426, doi:10.1038/nmeth762 (2005).
48 Perez, A. V., Perrine, M., Brainard, N. & Vogel, K. G. Scleraxis (Scx) directs lacZ expression in tendon of transgenic mice. *Mechanisms of development* **120**, 1153-1163 (2003).
49 Madisen, L. *et al.* A robust and high-throughput Cre reporting and characterization system for the whole mouse brain. *Nature neuroscience* **13**, 133-140, doi:10.1038/nn.2467 (2010).
50 Ackerman, J. E. & Loiselle, A. E. Murine Flexor Tendon Injury and Repair Surgery. *Journal of visualized experiments : JoVE*, doi:10.3791/54433 (2016).
51 Dyment, N. A. *et al.* High-Throughput, Multi-Image Cryohistology of Mineralized Tissues. *Journal of visualized experiments : JoVE*, doi:10.3791/54468 (2016).
52 Hasslund, S. *et al.* Adhesions in a murine flexor tendon graft model: autograft versus allograft reconstruction. *Journal of orthopaedic research : official publication of the Orthopaedic Research Society* **26**, 824-833, doi:10.1002/jor.20531 (2008).